Journal Pre-proof

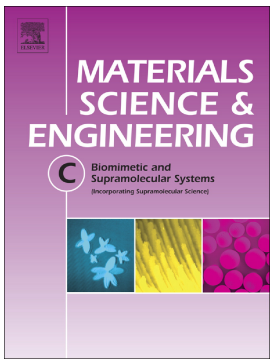

Effects of the sources of calcium and phosphorus on the structural and functional properties of ceramic coatings on titanium dental implants produced by plasma electrolytic oxidation

Sergiy Kyrylenko, Fiona Warchoł, Oleksandr Oleshko, Yevheniia Husak, Alicja Kazek-Kęsik, Viktoriia Korniienko, Volodymyr Deineka, Maciej Sowa, Artur Maciej, Joanna Michalska, Agata Jakóbik-Kolon, Izabela Matuła, Marcin Basiaga, Viktoriia Hulubnycha, Agnieszka Stolarczyk, Marcin Pisarek, Oleg Mishchenko, Maksym Pogorielov, Wojciech Simka

PII: S0928-4931(20)33525-6

DOI: https://doi.org/10.1016/j.msec.2020.111607

Reference: MSC 111607

To appear in: *Materials Science & Engineering C*

Received date: 11 August 2020

Revised date: 18 September 2020

Accepted date: 6 October 2020

Please cite this article as: S. Kyrylenko, F. Warchoł, O. Oleshko, et al., Effects of the sources of calcium and phosphorus on the structural and functional properties of ceramic coatings on titanium dental implants produced by plasma electrolytic oxidation, *Materials Science & Engineering C* (2020), https://doi.org/10.1016/j.msec.2020.111607

This is a PDF file of an article that has undergone enhancements after acceptance, such as the addition of a cover page and metadata, and formatting for readability, but it is not yet the definitive version of record. This version will undergo additional copyediting, typesetting and review before it is published in its final form, but we are providing this version to give early visibility of the article. Please note that, during the production process, errors may be discovered which could affect the content, and all legal disclaimers that apply to the journal pertain.

© 2020 Published by Elsevier.

Journal Pre-proof

Effects of the sources of calcium and phosphorus on the structural and functional properties of ceramic coatings on titanium dental implants produced by plasma electrolytic oxidation

Sergiy Kyrylenko[1], Fiona Warchoł[2], Oleksandr Oleshko[1], Yevheniia Husak[1], Alicja Kazek-Kęsik[2], Viktoriia Korniienko[1], Volodymyr Deineka[1], Maciej Sowa[2], Artur Maciej[2], Joanna Michalska[2], Agata Jakóbik-Kolon[2], Izabela Matuła[3], Marcin Basiaga[4], Viktoriia Hulubnycha[1], Agnieszka Stolarczyk[2], Marcin Pisarek[5], Oleg Mishchenko[6], Maksym Pogorielov[1,6,£], Wojciech Simka[2,6,*,£]

[1] Sumy State University, Medical Institute, 40018 Sumy, Ukraine

[2] Silesian University of Technology, Faculty of Chemistry, 44-100 Gliwice, Poland.

[3] University of Silesia, Institute of Materials Engineering, 41-500 Chorzów, Poland

[4] Silesian University of Technology, Faculty of Biomedical Engineering, 41-800 Zabrze, Poland

[5] Institute of Physical Chemistry PAS, 01-224 Warsaw, Poland

[6] Nano Prime, 39-200 Dębica, Poland

* Corresponding author: wojciech.simka@polsl.pl, Phone: + 48 32 237 26 05, Fax: + 48 32 237 2277

[£] Co-last authors

Keywords: dental implant, bioactive surface, anodization, osseointegration, hydroxyapatite, biocompatibility

Abstract

Plasma Electrolytic Oxidation (PEO) is as a promising technique to modify metal surfaces by application of oxide ceramic coatings with appropriate physical, chemical and biological characteristics. Therefore, objective of this research was to find the simplest settings, yet able to produce relevant bioactive implant surfaces layers on Ti implants by means of PEO. We show that an electrolyte containing potassium dihydrogen phosphate as a source of P and either calcium hydroxide or calcium formate as a source of Ca in combination with a chelating agent, ethylenediamine tetraacetic acid (EDTA), is suitable for PEO to deliver coatings with desired properties. We determined surface morphology, roughness, wettability, chemical and phase composition of titanium after the PEO process. To investigate biocompatibility and bacterial properties of the PEO oxide coatings we used microbial and cell culture tests. The electrolyte based on $Ca(OH)_2$ and EDTA promotes active crystallization of apatites after PEO processing of the Ti implants. The PEO layers can increase electrochemical corrosion resistance. The PEO can be potentially used for development of bioactive surfaces with increased support of eukaryotic cells while inhibiting attachment and growth of bacteria without use of antibacterial agents.

Journal Pre-proof

1. Introduction

Artificial osseous/dental implants have become a useful and reliable standard treatment option to replace tooth loss, as well as to repair bone defects [1-3]. The majority of the implants nowadays are fabricated using titanium and its alloys. Other materials, including non-metallic ceramic implants using zirconia (zirconium dioxide, ZrO_2) also show promises, but still lack long term clinical data to support their use despite showing advantages in short term applications [4, 5]. Titanium is an inert, light and mechanically stable metal, highly resistant to corrosion in

aggressive environments, including conditions prevalent in the human body, and is considered to be biocompatible. It has a very high weight-to-strength ratio, and is generally not immunogenic [6]. The main factors which determine the stability of the implant are i) the level of osseointegration, meaning ability to establish the direct firm contacts of the bone cells with the surface of the implants [7] and ii) the ability of the surface of the implant to resist bacterial colonization and formation of biofilms [8]. Another important factor is to maintain bone-to-implant contact over time during many years after surgery without intensive bone loss [9]. Certain conditions such as smoking, hypertension and diabetes negatively affect the success of dental implants [10]. Successful long time implant survival under such challenging conditions requires meticulous approaches to modify surfaces of the metal implants [11]. Sandblasting, acid-etching, hydrophilic surface textures, anodization and other approaches have been used to improve surface topography and to increase survival rate of the titanium implants [12].

Plasma electrolytic oxidation (PEO) has become a method of choice to deposit hard, durable and functional coatings on the metal surfaces [13, 14]. PEO setup is similar to anodization, with a difference of using a voltage high enough to break the dielectric barrier of the oxide layer and to start a dynamic process to form a relatively thick, hard and porous surface oxide layers. Primary factors which determine success of the PEO anodization are voltage, current density and electrolyte content. For successful osseointegration the surface layers should be non-toxic, non-immunogenic, resistant to corrosion and biocompatible. Furthermore, it is beneficial for the surface of the implant to have an optimal amount of hydroxyapatites, the main mineral component of the bone tissue [15]. As yet, there is no comprehensive understanding of the PEO process on different substrates under various conditions, and no exhaustive mathematical model of its mechanism has been built able to explain conversion of electrical

energy into chemical energy during the PEO process [16]. It has been shown that the various components of the electrolyte can impact the formation of the oxide layers and deposition of the desired components. Previously, electrolytes containing calcium and phosphorus have been used to treat metal specimens by PEO [17] and to incorporate such elements, namely Ca and P, into bioactive coatings. Studies have shown that the electrolyte components and their concentrations play a key role in determining the success of the PEO treatment [18].

The goal of this study was to find a simpler composition of PEO electrolytes containing Ca and P which would yield hard and porous bioactive surface coating on the titanium specimens. It is known that complex ions can be used for optimization of electrochemical performance of the PEO process [19]. In addition, EDTA, a strong chelating agent which binds various metal ions, has been shown to incorporate metal oxides into PEO coating due to the formation of the negatively-charged species [20]. Our study showed that bath electrolytes containing P and Ca in various forms combined with the EDTA provide optimal conditions to produce a functional bioactive coating on the titanium specimens, which can be used to manufacture dental/osseous implants. This will contribute to further understanding of the PEO process and, therefore, to build a comprehensive model of the molecular mechanisms of the PEO.

2. Materials and methods

2.1. Specimens. Commercially available pure titanium (Grade 4; IWET, Kleosin, Poland) was used to prepare experimental samples measuring 4 mm in length x 10 mm in diameter. Before the PEO process, the samples were polished using silicon carbide (SiC) paper rated at 400, 600 and 800 grit. The samples were then degreased in isopropanol in an ultrasonic bath for 3 minutes. Ethylenediamine tetraacetic acid (EDTA), calcium hydroxide ($Ca(OH)_2$), potassium dihydrogen

Journal Pre-proof

phosphate (KH_2PO_4) and calcium formate ($Ca(HCOO)_2$) were obtained from Chemia-Łódź, Łódź, Poland. All reagents used were in pure-for-analysis quality.

2.2. Plasma Electrolytic Oxidation (PEO). The Ti samples were subjected to PEO using a high-voltage power supply KIKUSIU PWR800H (Japan), which was controlled using a PC with Wavy software. The first stage of the study was the recording of curves (U, i) = f (t), in various bath compositions as shown in **Tab. 1**. The registration was carried out at three different fixed set current densities: 50, 100 and 150 mA cm^{-2}. The details of PEO treatment and samples post-treatment were described in [21].

The test samples as prepared above were used for further experimentation and were designated as following: Ti-X-Y-Z, where: X=bath number; Y=anodizing voltage; and Z=current density. For example, sample Ti-1-450-150 was anodized in electrolyte bath No. 1, with a final voltage of 450 V and a current density of 150 mA cm^{-2}.

TABLE 1

2.3. Scanning electron microscopy (SEM), and energy-dispersive X-ray analysis (EDX). Scanning electron microscopy (Hitachi S-3400N, Tokyo, Japan, accelerating voltage = 15 kV) was used for preliminary evaluation of surface morphology. SEM examination of chosen samples was made using Phenom ProX scanning electron microscope (accelerating voltage = 15 kV). Chemical composition of the surface layer was analyzed using energy-dispersive X-ray spectrometry (EDX, PhenomProX). Cross section was used to estimate thickness of the PEO coating layer formed on the substrate of Ti samples as described [22]. The size of the pores was calculated using Image J software [23].

2.4. Hydrophilicity, roughness, scratch test. The contact angle was measured as described in [22] using OCA 15 EC optical contact angle measuring and contour analysis systems (Data

Physics, Filderstadt, Germany) and distilled water. The roughness of the test material surfaces prepared by PEO was determined using Surftest SJ-301 profilometer (Mitutoyo, Japan). Adhesion of the oxide layer deposited on the surface of the Ti substrate during PEO and its mechanical stability was evaluated by a scratch test using an Open Platform equipped with a CSM Micro-Combi-Tester as described [24].

2.5. X-ray diffraction (XRD). All experiments were done using X'Pert Philips PW 3040/60 diffractometer, operated at 30 mA and 40 kV, equipped with a vertical goniometer and Eulerian cradle. X-ray diffraction pattern was registered in 2θ region: 10-140°using $CuK_{\alpha 1,2}$ radiation ($\lambda_{CuK\alpha 1}$ = 1.54056 Å and $\lambda_{CuK\alpha 2}$ = 1.54443 Å) for the incident α angle - 0.25 degrees (GIXD - Grazing Incidence X-Diffraction).

2.6. Raman spectroscopy. Measurement was performed on an inVia Renishaw Raman microscope equipped with a CCD detector using green (514 nm) laser excitation. Scans were taken on an extended range (100–35000 cm^{-1}). All measurements were made in a backscattering geometry, using a 50× microscope objective with a numerical aperture value of 0.75, providing scattering areas of ca 1 μm^2. Single point spectra were recorded with 4 cm^{-1} resolution and 30 s accumulation times.

2.7. X-ray photoelectron spectroscopy (XPS). The XPS analysis allows to characterize chemical composition and chemical state of the prepared samples. For this purpose, a PHI 5000 VersaProbe (ULVAC-PHI) spectrometer was used. The XPS spectra were excited using $Al_{K\alpha}$ ($h\nu$ = 1486.6 eV, 25 W) monochromatic radiation as a source. Details of the measurement and data analysis were described in [25].

2.8. Electrochemical corrosion resistance assay. Ability of PEO surfaces to resist corrosion was investigated using electrochemical methods. For this, the samples were mounted to the flat

corrosion cell (250 mL, Bio-logic, France) with the corrosion medium (Ringer solution with the composition: (8,6 g dm^{-3} NaCl, 0,3 g dm^{-3} KCl, and 0,48 g dm^{-3} $CaCl_2 \cdot 6H_2O$; Fresenius Kabi, Poland) at 37°C, via O-ring with the exposed surface area of 0.283 cm^2. Ringer's solution was kept in an incubator at 37.0 ± 0.5 °C before testing, to avoid precipitation bubbles of gas when heated in a corrosive cell to the measurement temperature. The three-electrode configuration was used with the reference electrode (saturated calomel electrode – SCE with Haber-Luggin capillary) and counter electrode (platinum). The experiments were performed using PARSTAT 4000A potentiostat-galvanostat (Ametek, Princeton Applied Research–Solartron, USA–the UK). The experimental procedure and the acquisition of data were realized using VersaStudio software ver. 2.60.6. The measurement procedure included i) open-circuit potential (EOC) stabilization for 1 h; ii) electrochemical impedance spectroscopy (EIS) at 10 mV RMS amplitude, in the frequency range of 39 810÷0.01Hz and 5 points per decade (experiment lasted 35÷45 min); iii) two potentiodynamic polarization (PDP) experiments after a short period of stabilization (5 min) which include a) short-range polarization at ± 40 mV vs. EOC, in order to obtain linear polarization resistance (LPR) of the sample, at a scan rate of 1 mV min^{-1}; b) long-range polarization at ±250 mV vs. EOC, in order to obtain information regarding the presence of Tafel regions and the passivation current densities, at a scan rate of 10 mV min^{-1}. The EIS data were further analyzed using complex non-linear regression least-squares fitting software (ZSimpWin ver. 3.60, Ametek, USA) with the use of appropriate electrical equivalent circuits (EECs) as mathematical models of the investigated electrochemical interfaces.

2.9. Incubation in Ringer's solution. The anodized samples were immersed in the flacons with the Ringer's solutions up to 12 weeks. The content of phosphorus and titanium in Ringer solutions after immersing test was determined using inductively coupled plasma atomic emission

Journal Pre-proof

spectrometry (ICP-AES) after each 2 weeks of the sample immersion. A Varian 710-ES spectrometer equipped with a OneNeb nebulizer was utilized. The parameters were as follows: RF power 1.0 kW, plasma flow 15 L min^{-1}, auxiliary flow 1.5 L min^{-1}, nebulizer pressure 210 kPa, pump rate 15 rpm, emission lines of P: λ=213.618, Ti: λ= 328.068 and 338.289 nm. The calibration curve was prepared based on the standard solutions for phosphorus and titanium in concentration of 1 mg mL^{-1} and 10 mg mL^{-1} in the Ringer's solution, supplied by Merck Millipore, Germany were used.

2.10. Simulated Body Fluid (SBF) bioactivity assay. Potential bioactivity of the samples was analyzed according to the standard procedure in simulated body fluid. The anodized samples were immersed in the SBF prepared as described [26]. One sample was immersed in 25 ml of the SBF solution, which was replaced every 3 days over 4 week period. The samples were shaken at 60 rpm at 37 °C. The morphology of the samples was analyzed after 1, 2, 3, and 4 weeks of immersion using the scanning electron microscope (Hitachi, TM-3000, accelerating voltage = 15 kV, BSE condition). For exemplary sample an EDX analysis was performed (PhenomProX; accelerating voltage = 15 kV).

2.11. Cytotoxicity and cell viability assays. Samples were sterilized in an autoclave at 121 ^{o}C for 1 hour and placed into 24-well plates. Each well was filled up with 20% of Fetal Bovine Serum (FBS; Invitrogen,) in Dulbecco's Modified Eagle Medium (DMEM; Invitrogen, cat. no. 11960) and left overnight in a cell incubator. This procedure was performed to mimic protein adhesion to implant surface after implantation. Next day the FBS solution was removed and 2 ml of DMEM supplemented with 10% FBS, 2 mM L-glutamine (Invitrogen, cat. no. 25030), 0.1 mM 2-mercaptoethanol (Sigma, cat. no. M7522), 50 units mL^{-1} penicillin and 50 g mL^{-1} streptomycin (Invitrogen, cat. no. 15070) was added to each well. Rat osteoblast (obtained from

Journal Pre-proof

cell collection of Sumy State University) at amount 10^5 cells were seeded on the top surface of each sample and incubated at 37 ºC in a humidified environment with 5% CO_2. Culture medium was changed every 3 days during a 7-day period. All experiments were done in triplicates. The following controls were employed: cell culture plate with cells but without the Ti specimen (TCP), reference sample – non-modified polished Ti specimen.

Resazurin reduction assay was used to access cell viability and proliferation rate on day 1, 3 and 7 after cell plating. Medium was removed from each well and washed with PBS twice. 1 ml of medium with 15 µg ml^{-1} resazurin was added to each well and incubated for 4 hours in cell incubator. Then, three aliquots of 200 µl of medium with resazurin were collected from each well and absorbance was red at a 570 and 595 nm in a colorimetric plate reader (Multiskan FC Microplate Photometer, Thermo Fisher Scientific). Cell viability, expressed as percent differences between cells with the PEO sample and control cells was calculated using formula from the Method for Measuring Cytotoxicity or Proliferation Using AlamarBlue by Spectrophotometry (BioRad): ((O2 x A1) - (O1 x A2)) / ((O2 x P1) - (O1 x P2)) x100, where O1 = molar extinction coefficient (E) of oxidized resazurin at 570 nm (80586) , O2 = E of oxidized resazurin at 595 nm (117216), A1 = absorbance of test wells at 570 nm, A2 = absorbance of test wells at 595 nm, P1 = absorbance of positive growth control well (cells plus resazurin but no test specimen) at 570 nm, P2 = absorbance of positive growth control well at 595 nm.

To obtain information about cell adhesion and distribution on day 7 over the implant surface, samples were fixed with 2.5% glutaric aldehyde and subjected to osmium coating for 1 h, then washed three times in 0.1 M cacodylate buffer. Samples were then dehydrated in increasing ethanol concentrations (70-100%), sputtered with gold and observed in the SEM (Hitachi, TM-3000, accelerating voltage = 15 kV, BSE condition).

Journal Pre-proof

2.12. Bacteria adhesion assay. A suspension of overnight culture of *Staphylococcus aureus* (B 918), obtained from the National Collection of Microorganisms (Institute of Microbiology and Virology NASU, Kyiv, Ukraine) was mixed with nutrient media to concentration of 10^8 by McFarland scale using densitometer DEN-1B (Biosan SIA, Latvia) and a final concentration of microorganisms was adjusted to 10^5 CFU ml^{-1}. Untreated Ti (reference) and PEO coated samples were placed into sterile polystyrene 24-well plates and covered with 2.0 ml of the bacterial suspension. After incubation at 37°C for 2, 4, 6 and 24 hours, the disks were rinsed with sterile sodium chloride solution three times to remove all bacterial cells unattached to the surface of the test samples. Subsequently, the test samples were placed individually in a test tube containing 1.0 ml of sterile saline solution and subjected to ultrasonication (B3500S-MT, Branson Ultrasonics Co., Shanghai, China) for 1 minute to dislodge the bacteria attached to the surfaces of the specimens. 10 µl aliquots of the saline suspension were then plated onto nutrient agar using streak plate technique to count the total number of bacteria after incubation at 37°C for 24 hours.

2.12. Statistical analysis. One way analysis of variance (ANOVA) was used for the data analysis, if not otherwise specified. All tests were carried out in triplicates for each time point. The data were expressed as means ± standard deviation. Statistical significances was indicted with asterisks where * means $p \leq 0.05$, ** - $p \leq 0.01$ and *** - $p \leq 0.001$.

3. Results

3.1. Voltage vs current as a function of time. Analysis of the curves (U, i) = f (t) show that the PEO process of Ti in baths containing a combination of complexing agent (EDTA) and calcium hydroxide did not produce the desired results (data not shown). The curves indicate an unstable process, and the set final voltage was not achieved within 5 minutes. Increasing the process time

Journal Pre-proof

did not give satisfactory results either, as the voltage was very low. Results were the same regardless of the calcium salt used (calcium hydroxide or calcium formate) as a source of calcium ions (data not shown). As in the previous case, the recorded curves were "jagged" and the voltage did not rise to the set level. However, addition of KH_2PO_4 as a source of P to the bath resulted in the PEO process on Ti samples to proceed (**Supplement Fig. 1**). Each of the curves for baths 1-2 and 3-4 looked similar, regardless of the current density used. At the beginning of the process, the voltage increased linearly depending on the current density. The higher the current density, the faster this process proceeded. Then, after reaching the breakdown voltage of the oxide film (process in the PEO regime), the rate of increase of voltage was reduced and lost its linear character. The breakdown voltage of the oxide film depended mainly on the chemical composition of the bath used. On the recorded curves (U, i) = f (t) there are the points of inflection at which the rate of voltage increase changes. The presence of these points results from a change in the mechanism of formation of the oxide layer on Ti, as well as from a change in its physical and chemical properties (thickness, composition). At this point, the process started to show electric discharges (sparks) on the surface of Ti.

Depending on the chemical composition of the bath and the current density, different end point voltages were obtained. The rate of reaching the final voltage depended on the current density used. It should be noted that about 500 V voltage was obtained only using the current density of 150 mA cm^{-2}. The voltage was selected such that it was in the middle of a given range in which the process proceeded according to one oxidation mechanism. Based on the analysis of the curves (U, i) = f (t), particular parameters of the voltage and current density for PEO on Ti samples were selected for further studies.

Journal Pre-proof

3.2. SEM analysis. Fig. 1 shows representative SEM images of titanium samples subjected to PEO in selected solutions (please refer to **Supplement Fig. 2** for a complete set of SEM images with the electrolytes 1, 2, 3 and 4). The selection of oxidation parameters was made on the basis of previously registered curves (U, i) = f (t). The images were analyzed for the quality of the surfaces obtained, as well as potential use as target coatings on dental implants. Such coatings should possess a porous structure free of cracks.

Electrolyte 1: regardless of the parameters used, a relatively thin oxide film was formed on the titanium surface. This is evidenced by the scratches visible on almost all surfaces, which are the remnants of the grinding of the samples. Only at 450 and 500 V (j = 150 mA cm^{-2}) formation of pores is clearly observable. Therefore, samples Ti-1-450-150 and Ti-1-500-150 were selected for further research.

Electrolyte 2: at voltages below 400 V, the surface morphology is similar regardless of the current density used. The PEO coating is thin, with few pores and sandblasting scratches visible. Increasing the voltage to 400 V resulted in the formation of a thicker oxide film and the disappearance of grinding scratches. The reach porous surface morphology of the obtained oxide films typical for the PEO process is visible. As a result, the following samples were selected for further analyses: Ti-2-400-100, Ti-2-400-150, Ti-2-450-100 and Ti-2-500-150. Due to the similarity of the structures of the oxidized sample at 450 V and the two current densities of 100 and 150 mA cm^{-2}, the lower current density was chosen. Generally, at lower current density, milder oxide films are produced, which can lead to a reduction of internal stress in the oxide layer diminishing probability for formation of cracks.

Journal Pre-proof

Electrolyte 3: regardless of the applied parameters of sample processing, each surface looked very similar. The coatings produced mostly reflected the surface of the titanium substrate. At higher voltages, coatings with fine pores were visible.

Electrolyte 4: clearly porous coatings were obtained only when using a current density of 150 mA cm^{-2} and a voltage above 350 V. However, the obtained coatings did not differ in any way compared to the previously selected ones.

FIGURE 1

FIGURE 2

Fig. 2 show distribution of pore size in corresponding samples. The overall trend was visible to increase the size of the pores with increased volt-ampere characteristics. Sample Ti-1-450-150 has the smallest pores, majority of which have size around 2 μm. On the other hand, the sample Ti-2-500-150 shows classical bell shaped distribution, where the majority of pores have 3-4 μm in size.

3.3. EDX analysis. The PEO layer on the sample Ti-1-450-150 was slightly enriched with P and Ca (**Fig. 3**), the components of the bath electrolyte (peaks with low intensity visible on the EDX spectrum). In the sample Ti-1-500-150 the surface is more developed and porous than on the Ti-1-450-150, and the oxide layer has been enriched to a greater extent with the bath components P and Ca. Peaks for oxygen and titanium, components of the oxide film, are also visible in both samples.

FIGURE 3

The oxide layer on the sample Ti-2-400-100 was significantly enriched with the bath components P and Ca. Noteworthy is the high intensity of the phosphorus peak. Increasing the current density from 100 to 150 mA cm^{-2} clearly increased the content of calcium and

phosphorus in the oxide film (sample Ti-2-400-150). Increasing the voltage to 450 V, at a density of 100 mA cm^{-2}, did not increase further the content of Ca and P in the oxide film. Increasing the voltage to 500 V and at the same time the current density to 150 mA cm^{-2} caused a very substantial development of the titanium surface, as well as considerable enrichment of the oxide layer with bath components. Thus, in both samples Ti-2-400-150 and Ti-2-500-150 the oxide layers were enriched with the bath components P and Ca. The oxide layer was thicker in the former sample (as shown in section 3.4), while the structure of the coating was more favorable in the latter. In all the samples tested, the EDX spectrum also showed peaks of oxygen and titanium, the components of the oxide film. These results imply that both PEO protocols used to generate oxide coatings on the samples Ti-2-400-150 and Ti-2-500-150 can be employed to produce coatings highly enriched with Ca and P, the constituents of the hydroxyapatite; while fine tuning of the PEO parameters is still required for elucidation of the most optimal conditions for generating surface layers with potential propensity for osseointegration.

3.4. Analysis of cross sections. An exemplary SEM image of cross-section as well as EDX mapping of Ti sample after PEO process is shown in **Fig. 4**. Based on the analysis of cross-sections of oxide layers produced on titanium and their EDX mapping, it was found that regardless of the process parameters used, the obtained coatings adhere well to the base material. We noticed that layer detachment was occasionally observed only as an artifact during sample preparation. The thickness of the coatings did not exceed 6 μm. The EDX mapping of oxide layers confirmed that, in each case, the elements contained in the electrolyte bath (Ca and P) were incorporated into the entire structure of the oxide layer.

FIGURE 4

Journal Pre-proof

3.5. X-ray photoelectron spectroscopy (XPS). XPS is a very sensitive research technique, which allows to accurately determine the concentration of chemical elements on the surface, as well as to assign chemical states to these elements. The XPS investigations revealed that after PEO treatments the surface of Ti forms the layer which consists of a mixture of oxides and phosphates. The exemplary spectra from samples Ti-1-450-150 and Ti-2-500-150 after deconvolution procedure, including values for P2p, Ca2p, C1s, K2p, Ti2p, O1s and N1s are shown in **Supplement Fig. 3**. Four chemical states of oxygen were separated in O1s spectra recorded for both samples. The first one at 531.3 eV or 531.4 eV is attributed for oxygen in calcium phosphate functional groups (PO_4^{3-}) [27], the second state at BE of 530.2 and 530.4 eV can be dedicated to Ti in TiO_2 lattice [28], the third and fourth states are assigned to bonds C=O and C-O [27], the second state at BE of 530.2 and 530.4 eV can be dedicated to Ti in TiO_2 lattice [27,28]. The high-resolution XPS spectra of P2p shows a main peak at 133.3 and 133.4 eV, which correspond to calcium phosphate chemical states [27,29] and component at higher binding energies, which is probably attributed to the hydrogen phosphate (134.4 eV, HPO_4^{2-}) [28]. The Ca2p spectra confirm the presence of calcium phosphate in the layer, where the characteristic $Ca2p_{3/2}$ peaks were detected at 347.5 and 347.6 eV [28,29]. For the sample Ti-2-500-150 the XPS also revealed the presence of potassium, which was associated with the PO_4^{3-} groups ($K2p_{3/2}$ - 292.9 eV) [30]. The representative $Ti2p_{3/2}$ peaks at binding energy of 458.8 and 459.1 eV are characteristic for Ti in TiO_2 structure and can be identified as Ti^{4+} [27,28]. The nitrogen chemical species were also detected in the XPS spectra. Two similar chemical states of nitrogen were separated after deconvolution of N1s spectra for investigated samples. The signals at 399.9 and 401.1 eV were assigned to amino groups ($C\text{-}NH_2$), while the second at 401.9 eV to amide groups ($C\text{-}NH_3^*$). These findings could also be seen in the C1s spectra where three carbon states

were distinguished at: 284.8 eV (C-C), 286.4 – 286.5 eV (C-O; C-N), 288.8 – 288.9 eV (O=C-OH, N-C=O) [28].

As a result, in all samples tested only the PEO process-related elements were detected, which indicates the purity of the material used. No impurities were detected. The only foreign element was silicon, which was a result of carry-over from the grinding process of the samples. The highest oxygen concentration was recorded on the surface of samples, as expected. Its content ranged at 40-60% (**Tab. 2**). Oxygen was mainly found in the form of titanium oxide, but also in the phosphate form and in compounds with carbon. Oxygen and carbon compounds were derived mainly from the complexing agent used (EDTA). The content of phosphorus ranged at 8-14%. P was present only in the phosphate form (PO_4^{3-}), as in calcium and potassium phosphate. This element derived from the electrolyte bath. Another important element, calcium, was present in each of the samples tested. Its content ranged at 0.5-9%. Calcium was found only in the form of calcium phosphate. This compound was formed during the anodic oxidation of titanium. It derived from the Ca-EDTA complex. Potassium, another component of the bath, very poorly incorporated into the oxide layer. Its content oscillated at 0-0.2%, mainly in the phosphate form. Titanium, with the content at 10-15%, was found mainly in the oxide form. Remarkably, nitrogen was also detected at the oxide layer. It derived from the Ca-EDTA complex. Nitrogen content was relatively low, not more than 2%, and it occurred in the form of amino groups linked to carbon. Despite the low content, nitrogen can add substantially to the combination of chemical factors which drive to biocompatibility. These results point that the PEO conditions used to generate the sample Ti-2-500-150 were adequate for obtaining biologically active surface layers.

TABLE 2

Journal Pre-proof

3.6. Raman spectroscopy. Analysis of Raman spectra allows us to state whether there is well-crystallized TiO_2 in the form of anatase (narrow signals at 144; 390; 512; 633 cm^{-1}) on the tested surfaces. For some of the samples, wide signals of phosphorus groups (260; 800; 1006 and 3132 cm^{-1}) (calcium phosphate), indicative of high amorphicity, were recorded. **Fig. 5** shows the spectra of the samples with different phosphate contents. Analysis revealed that the surfaces of all tested samples contain crystallized TiO_2 in anatase form. In addition, in some of the samples, wide signals of phosphorus groups (calcium phosphate) were found to be highly amorphous. Different phosphate content was in different samples. The content of phosphate groups in relation to titanium dioxide was estimated by determining the ratio I_{1006}/I_{144} (**Tab. 3**). The values were generally lower for PEO samples obtained with electrolyte 1 and higher for electrolyte 2. The lowest phosphate content was recorded for the Ti-1-500-450 sample and the highest for Ti-2-500-150. No additional signals from EDTA were registered. Therefore, the PEO protocol with electrolyte 2, voltage 500 V and current density 150 mA cm^{-2} can be optimal for obtaining surface layers with high phosphate content, and therefore with potential propensity for osseointegration.

FIGURE 5

TABLE 3

3.7. XRD data. GIXD uses small incident angles (α) for the incident X-ray beam, so that it is used to study surface layers as the beam penetration is limited. Distances are in the order of nanometers. The α angle of incidence is fixed, so that the degree of penetration by the X-rays into the sample remains constant throughout the measurement. At low α-angles of incidence, the X-rays penetrate only the uppermost layers of a sample. The diffraction patterns (α = 0.25) of the samples show that the layers have a polycrystalline character. In addition, for parts of the

Journal Pre-proof

samples (Ti-2-400-100, Ti-2-400-150), amorphous 'hallo' is visible (**Fig. 6**). Phase analysis of samples shows that the layer is composed of TiO_2 [anatase, s.g. I41/amd] (ICDD PDF 01-084-1286) and Ti [alpha titanium, s.g. P63/mmc] (ICDD PDF 01-089-5009) phases. In the case of Ti-10-500-150 sample TiO_2 [Rutile, s.g. P42/mnm] (ICDD PDF 04-007-5403) phase is also observed. At XRD spectra Ca nad P compound are not visible. The reason is that Ca-P phase is amorphous or nano-crystaline (visible as the 'hallo' effect on the XRD spectra).

FIGURE 6

3.8. Roughness and hydrophilicity of the PEO surfaces. Roughness of the PEO surfaces was revealed to be generally higher for the electrolyte 2 in comparison to electrolyte 1, and was the highest for the sample Ti-2-500-150 (**Fig. 7**). Higher roughness can facilitate attachment and proliferation of the osteogenic cells [31]. Therefore, the PEO protocol used to generate sample Ti-2-500-150 was optimal for formation of potentially bioactive and biocompatible surfaces on Ti implants with possible propensity for osseointegration.

FIGURE 7

Measurement of contact angle revealed that PEO treated surfaces of the Ti samples acquired substantially higher hydrophilicity in comparison to the reference Ti samples without any PEO surface (**Fig. 7**), in concordance with the previously reported results [20]. This suggests that the PEO generated surfaces can be regarded as more bioactive in comparison to the untreated titanium.

3.9. Scratch test. Scratch test is an accepted method to estimate interfacial adhesion of a coating layer to the underlying substrate material. The critical load Lc is the normal force applied to the penetrator causing the interfacial failure to occur, which correlates to the adhesion strength. Continuous plastic perforation of the layer was detected in every sample tested (**Fig. 8A**). The

Journal Pre-proof

value of the critical load Lc1 corresponds to the onsets of adhesive failure when cracking starts; while the Lc2 corresponds to the onset of spallation (breaking-up) of the adhesive layer (**Supplement Fig. 4**). Different values of critical force Lc1 and Lc2 were detected depending on the PEO parameters (**Fig. 8B**). It was found that the sample Ti-2-400-100 had the strongest adhesion, with the value of the critical force Lc2 = 9.01. In every sample tested, no acoustic emission was detected, which indicates that the ceramic coatings were not brittle. Moreover, different values of critical force were observed for the different samples, due to their various thicknesses and probably their various porosity. It can also be interpreted as information about the internal structure of the various layers, which might have more porous areas inside, thus the intender penetrates the layer faster, which in turn is connected with the brittleness of the layers.

FIGURE 8

3.10. Resistance to electrochemical corrosion. Electrochemical corrosion assay was used to evaluate the corrosion behavior of the PEO-treated Ti (**Fig. 9)**. The results show that the spectrum for the reference sample (non-treated Ti) is characterized by a single time constant. On the other hand, the spectra of the PEO treated Ti had at least two times constants (**Fig. 9B**). Furthermore, the spectra measured for these samples had the overall impedance higher than that of the reference sample over the entire investigated frequency range (**Fig. 9A**). In all of the EECs presented, capacitances were approximated by the use of constant-phase elements (CPEs).

For the fitting analysis of the bare Ti sample (reference sample), a typical $R_s(Q_{bar}R_{bar})$ circuit has been selected. R_s stands for the resistance between the reference electrode (RE) capillary tip and the surface of the sample (working electrode - WE). R_{bar} is the interfacial resistance associated with the presence of the barrier passive oxide layer on the substrate.

FIGURE 9

Journal Pre-proof

Q_{bar} approximates the capacitive effects corresponding to the passive oxide layer. The impedance response of the PEO-treated titanium samples has been modeled by the use of an EEC shown in **Fig. 9C**. The resistances corresponding to the impedance response of the outer porous (R_{po}) and inner barrier (R_{bar}) layers of the PEO were taken into account for this type of samples. The role of Q_{coat} was to model the capacitance of the whole coating (porous + barrier layers), while the Q_{bar} refers to the capacitive behavior of the inner barrier layer. To properly fit the experimental results to the equivalent circuit, the authors needed to incorporate another element to the EEC. Therefore, the authors have decided to include a semi-infinite diffusion Warburg impedance (W) circuit element in the analysisfor the diffusion of the corrosive medium through the porous architecture of the coating [32, 33].

TABLE 4

The results of the fitting are summarized in **Tab. 4**. It can be noted that the n parameters of the CPEs in the circuits range between 0.77 and 1.00 which is typical for the capacitive elements of the corrosion systems. In addition, Ti-1-450-150 and Ti-1-500-150 samples had very similar corrosion properties with the latter being slightly less resistant. Moreover, the resistance of the porous portion of the coating was higher for the sample PEO-ed at 500 V suggesting that either its thickness was higher than that of the sample treated up to 450 V or its porosity was lower. This finding is in line with the higher value of the Warburg coefficient determined for the Ti-1-500-150 sample. As seen from **Fig. 9**, the fit parameters (**Tab. 4**) of the samples treated in the solution no. 2 show that their corrosion resistance was superior to the PEO treated Ti samples obtained in the bath no. 1. The R_{po} values for this series of samples were an order of magnitude higher than that for the Ti-1-450-150 and Ti-1-500-150. The best results were obtained for the Ti-2-400-150 sample, while corrosion resistance of the other Ti samples was only slightly lower.

Journal Pre-proof

TABLE 5

The results of the long-range PDP scans are presented in **Fig. 9D**, while the corrosion parameters extracted from the DC experiments can be found in **Tab. 5**. It can be noted that the anodic branch of the Tafel plot corresponding to the bare Ti surface (**Fig. 9D**) the oxidation of the metal occurs. In such conditions, the oxidation results in the passivation of the metal [34]. However, the characteristic plateau, in which the passivation current density (i_{pas}) could be assessed, has not been reached at the potential range selected in this study. Therefore, in this work, i_{pas} was chosen to be the current density measured at the terminal potential of the scan (at +250 mV vs. E_{OC}). Nevertheless, in the case of all of the PEO-treated samples, the passivation plateau was reached almost immediately after passing through the corrosion potential (**Fig. 9D**). By following the data in **Fig. 9D** and **Tab. 5**, the same conclusion as in the case of the EIS analysis (**Fig. 9A-C**, **Tab. 4**) can be made that the best performing Ti sample was the Ti-2-400-150 (the highest R_p and the lowest i_{pas}). However, the corrosion resistance of the other PEO-treated samples was still much higher than of the bare Ti sample. Additionally, the E_{cor} of these samples was shifted towards more positive values with respect to the reference. Overall, this shows that the corrosion resistance of Ti was improved by the PEO treatment, regardless of the conditions employed, with the highest values obtained for the Ti-2-400-150 sample.

3.11. Long term corrosion resistance assay (in Ringer's solution). Corrosion was investigated by prolonged exposure in Ringer's solution for 12 weeks at 37 ^{o}C with constant agitation. The release of Ti, Ca, and P into the fluid was measured by ICP-OES. The **Fig. 10** shows dynamics of release of Ti and P into the Ringer's solution during exposure for 12 weeks. The measurement of the release of Ca did not show invariable data in comparison with the control Ringer's solution values (not shown). The results revealed that the non-treated Ti surface did not release detectable

Journal Pre-proof

amounts of Ti ions (below 0.01 mg L^{-1}) throughout the duration of the experiment. However, treated samples indeed showed the appearance of Ti ions in corrosion solution. Notably, the sample Ti-2-400-150 released the highest amount of the Ti ions.

FIGURE 10

3.12. Potential bioactivity of PEO generated surfaces in SBF assay. Simulated Body Fluid assay was used to reproduce the effects of body fluids on the surface layers of the PEO generated test samples with respect to crystallization of apatites. The samples were exposed to SBF solution for 4 weeks and the surface morphology was observed after each week (see **Supplement Fig. 5** for the complete list of SEM images). We observed the following phenomena (**Fig. 11**):

Ti: As expected, no increase of any apatite precipitation was detected on the surface of titanium for 4 weeks of exposure in SBF solution.

Ti-1-450-150 and Ti-1-500-150: minimal precipitations were detected on the sample surfaces after the second week of exposure, which did not increase with time. We concluded that these surfaces are indifferent to the process of crystallization of apatites.

Ti-2-400-100: the sample surface was completely covered with a layer of apatites after two weeks of exposure. The layer was thick enough that after a few weeks it detached and fell off the surface of the samples. It suggests that this particular surface promotes crystallization of apatites.

FIGURE 11

Ti-2-400-150: a clear crystalline layer was visible on the surface after two weeks of exposure. At the end of the third week, the entire surface was covered with a thick layer of apatite which started to crack. This layer eventually detached and fell off the sample the

following week. We concluded that this surface has high potential to promote crystallization of apatites.

Ti-2-500-150: minor amount of precipitates were detected on the sample surface, which did not increase with incubation. Obviously, this surface does not promote the process of crystallization of apatites.

Overall, these results show that the electrolyte bath solution number 2 actively promotes crystallization of apatites after PEO processing of the Ti implants. Furthermore, the test sample Ti-2-400-150 appears to have the surface properties to induce high degree of bioactivity. The rate of crystallization however should be carefully controlled as too thick apatite layers have limited mechanical stability and are prone to self-detachment.

An XRD analysis and an EDX analysis of oxidized titanium surfaces after exposure in a simulated physiological solution were performed. Phase composition was evaluated by XRD assay with a Cu lamp and a nickel filter. Samples Ti-2-400-100 and Ti-2-450-150 were chosen because formation of apatite layer on their surfaces after immersion in simulated body fluid was preliminary observed. Images in **Supplement Fig. 7** show the diffractograms recorded for the Ti-2-400-100 (II week) and Ti-2-450-150 (III week) samples, for which an analysis of the phase composition of the coating in the 2Theta 20°-40° angle range was performed. No characteristic diffraction reflections clearly indicating the presence of a phase containing hydroxyapatite were recorded for the above samples. In the angle range of 25°-27° 2Theta and 31°-34° 2Theta indicates the presence of an amorphous phase, which may indicate the presence of titanium oxide as well as the formation of an amorphous phase containing calcium phosphates as a result of surface immersion in the SBF solution. In addition, no signals characteristic for titanium oxide in the polymorphic form of anatase or rutile were recorded in the studied range, hence it can be

Journal Pre-proof

concluded that the recorded amorphous area was registered for the formed apatite part. The characteristic diffraction reflexes corresponding to the titanium-containing phase were recorded. The presence of calcium phosphate is indicated by the surface morphology on which the formation of the apatite layer has been confirmed wit use of the EDX method (**Fig. 12.**). On a spectra clearly visible are peaks from Ca, P and O (O not marked). An atomic ratio of calcium and phosphorus (Ca/P) is around 1.68. This value is very characteristic for the hydroxyapatite. Therefore, the PEO surfaces generated with the bath electrolyte 2 can have propensity to form hydroxyapatites under physiological conditions in the body.

FIGURE 12

3.13. Cytotoxicity and cell viability assays. The resazurin reduction assay at day 1 shows primarily the level of specimen cytotoxicity and cell attachment, as proliferation is not yet intensive during this short period of time. As seen from the **Fig. 13**, all tested PEO surfaces were favorable for cell viability and did not show any signs of cytotoxicity. Cell attachment was better in all PEO samples tested in comparison to the reference (polished Ti surface without any PEO layer). Among the various test samples, Ti-1-450-150, Ti-2-400-100 and Ti-2-500-150 showed significant superiority over others in cell attachment at the end of one day incubation. No major difference was observed between all samples tested at day 3. Some samples showed retarded growth after 7 days of incubation. It is possible that at this time point the conditions were not favorable for proper estimations due to overgrowth of the cells.

FIGURE 13

FIGURE14

Scanning electron microscopy demonstrates uniform osteoblast cell distribution on the specimen surfaces (**Fig. 14**). The cells are aligned and evenly distributed on all Ti-1 samples, as well as on

the Ti-2-440-100 and Ti-2-400-150. Both Ti-2-400-100 and Ti-2-500-150 have random cell distribution with lower cell numbers. Despite differences in cell distribution, they both have acquired conventional elongated shape and numerous contacts. Low cell density on Ti-2-500-150 sample on day 7 correlates with resazurin reduction assay data and may suggest adhesive surface properties after seeding the osteoblasts.

3.14. Bacteria adhesion assay. Long term survival of the dental implant depends on its ability to resist bacterial adhesion on its surface followed by colonization and formation of biofilm. The objective of the bacteria adhesion experiment was to determine the abilities of the PEO generated surfaces to resist adherence of bacterial cells. Bacterial adhesion using *Staphylococcus aureus* was determined after 2, 4, 6 and 24 h exposure of the test samples to the microorganism. After 2 h incubation only Ti-2-400-150 was found to contain significantly less bacteria adhering to the surface compared to non-treated Ti sample (**Fig. 15**). When examined at 4 and 6 hours, no significant differences were found for bacterial adhesion to the surface between all the test samples vs. control. However, after 24 hour incubation period, samples Ti-1-500-150 and Ti-2-400-100 revealed significantly less bacteria adhered to the surface vs. control. Therefore, under these experimental conditions the PEO generated surface layer on the Ti-2-400-150 was effective to resist bacterial attachment over short term while both Ti-2-400-100 and Ti-1-500-150 were effective to resist bacterial adhesion over long duration.

FIGURE 15

4. Discussion

Our objective was to find a simple composition of PEO electrolyte which can form a desirable coating layer on the surface of the Ti implants. Recent report showed that acid etching technique did not produce Ti surfaces with roughness suitable to support cell proliferation [35]. Bioactive

coatings were successfully synthesized by PEO in electrolytes with both basic and acidic pH [36]. The presence of certain specific chemical groups can lead to increased propensity to bind particular proteins and to form firm bonds with osteogenic cells [37]. The ability of the surface coating to support biological functions, e.g. osteoinduction and osseointegration, is determined by the similarity of its structure and its chemical composition to the biological tissues. The main mineral component of the bone is hydroxyapatite, which consists of Ca phosphate, $Ca_5(PO_4)_3(OH)$. Therefore, to have a propensity to osseointegration, the surface layers of an implant need to maintain Ca phosphate groups, which can facilitate bonding with the bone tissue. We thus hypothesized that phosphate can be added to the electrolyte using potassium phosphate, KH_2PO_4. In addition, the electrochemical parameters (voltage/current) during PEO without KH_2PO_4 did not reach expected stable behavior (data not shown). As to the source of calcium ions to form calcium phosphate complex, we investigated two options: an inorganic and an organic source of calcium, namely calcium hydroxide, $Ca(OH)_2$ and calcium formate $Ca(HCOO)_2$ (**Tab. 1**). Based on our previous observations and the results of others, we postulated that calcium ions should preferably be supplied in the form of a large organic complex. Thus, we furnished the bath electrolyte with ethylenediamine tetraacetic acid, a chelating agent which binds various metal ions and was previously shown to incorporate metal oxides into PEO coating due to the formation of the negatively-charged species [19, 20]. In addition, presence of the metal-EDTA complexes led to reduction in open porosities in the coating layer. It was also suggested that the use of EDTA and metal-EDTA complexes as electrolyte additives can be helpful to reduce the defects formed in PEO coating layer without the use of complicated current waveform and an extended coating time [19]. This was in line with the proposed model for mechanisms of deposition of calcium phosphates during the PEO

Journal Pre-proof

process [7, 38]. An important parameter for osseointegration is the ratio of Ca/P in the coating surface. Thus, growth of endothelial cells was higher on the coating with the highest Ca/P ratio [39]. In addition, the most optimal growth condition for osteoblasts occurred at Ca/P ratio around 1.7 in bulk Ca-P materials [40, 41]. Although our PEO coatings have Ca/P ratios not higher than 0.26 judged by the XPS analysis (**Tab. 2**), they however showed substantial ability for deposition of apatites when subjected to simulated physiological conditions within the body, as supported by the SEM images after incubation in SBF (**Fig. 11**) and confirmed by the EDX assay (**Fig. 12**). Importantly, the SBF assay with non-coated Ti did not show any increase in apatite precipitation after prolonged 4 week exposure in SBF solution. On the contrary, the PEO surfaces induced robust precipitation of apatites, which often resulted in self-detachment (delamination) of the apatites, occurred between 3 and 4 week of exposition. This suggests that ability of the PEO generated layers to induce apatite precipitation needs to be carefully balanced to achieve a desired coating, as too thick a layer of apatites could compromise mechanical stability of the bioactive surfaces. The mechanism of deposition of apatites is a multistage process, based on a specific adsorption of Ca ions on negatively charged surface and continuous adsorption of phosphate ions on adsorbed Ca. It can be noted here that the results of SBF tests were not always unambiguous and sometimes were in disagreement with the results of the biological assays, e.g. an inactive surface in SBF solution can show high activity in biological (cellular) assays and vice versa. These discrepancies require further investigations. However, in general our results suggest that the PEO coatings increase potential propensity of the implants for osseointegration due to its increased Ca/P content.

The surface-to-bone interface of an implant is the basis of the interaction between the material and the bone tissue [42], and the size and morphology of the pores of the implants play

major roles in their biocompatibility and their propensity for osseointegration. Biomimetic coatings show their osseointegrative properties in large part due to the optimal distribution of the pore sizes [43]. Thus, pores less than 120 μm in size have been considered substantially smaller than those required for osteoblast penetration [44]. We showed that PEO can be a method of choice to generate microporous biomimetic coatings for its ability to form pores of the optimal size (**Fig. 1**). It was reported that also the ultrafine (100 nm) pores can participate in enhancing cellular responses [45]. The size of the pores and their morphology play a role in defining biological properties of the implants and their surfaces. It was reported that bioactive surface coatings which possess a microporous structure with pore size of 3-4 μm in average diameter, the same as in the sample 2-500-150, exhibit high osteogenic and angiogenic activities [46]. Detailed analysis of the SEM images revealed that PEO parameters used to obtain the surface layer on the sample Ti-2-400-150 can provide optimal conditions for generating Ti coatings suitable for manufacturing dental (osseous) implants. In general, increase in the voltage and current led to more structured surface morphology (**Fig. 1**) and thicker layers. When the voltage-current parameters reached optimum, the surface layers did not show any longer the background lines remaining from the polishing process. Then, with increasing the voltage-current further, the dynamic process of forming the oxide coating becomes suboptimal, yielding larger pores, most probably interconnected, and thinner oxide layers. To determine the integrative optimum of the PEO parameters requires taking into account data from various assays based on different nature. Thus, porosity, layer strength/brittleness, corrosion resistance, etc. all have to be considered for use practical optimum of the PEO parameters. We speculate that optimal conditions lie between 400-500 V voltage and 100-150 mA cm^{-2} currents in bath electrolyte no. 2. In general, the osseointegrative capacity of the implants depends on many factors, including coordination,

covalent bonding, electrostatic interactions, hydrogen bonding, etc. [47] and abilities e.g. to support specific protein absorption and formation of filopodia by surrounding cells and their firm attachment to the surfaces [46]. It still remains elusive which surface features are more effective in regulating cell functions [45]. We however suggest that optimal results for long term stability of the implants will most probably be accomplished using combination of both microporous coatings with macroporous structure of the implants, which can be achieved by e.g. additive manufacturing or powder metallurgy [48] followed by PEO processing. Further efforts are to be invested into generating bioactive surfaces with due porosity for optimal osseointegration capacities.

The biocompatibility of the coatings depends also on their hydrophilicity. The PEO coatings generated with all bath electrolytes tested showed preferential wettability, based on contact angle assay with water (**Fig. 7**). All test samples were found to have a contact angle of 40^{o} or less, suggesting the surface is highly hydrophilic vs. control, untreated Ti which showed a value of >90 degrees. It shows that PEO process greatly enhances the biocompatibility of the surfaces.

Dental/osseous implants are supposed to withstand high mechanical loads, and therefore are required to possess relatively high compressive strength [44-51]. We have investigated both the mechanical stability and adhesion strength of the PEO layers via scratch test (**Fig. 8**). The scratch test suggested that the PEO is a promising technique to obtain surface layers with the intended mechanical characteristics, while further studies are needed to investigate how the PEO layers with the desired adhesion strength and internal substructures can be built.

Chemical characterization of a sample by EDX analysis (**Fig. 12**) revealed that the PEO coatings were significantly enriched with the bath components P and Ca, the main constituents of

Journal Pre-proof

the hydroxyapatite, which is in line with the results of SEM, XRD and Raman analyses. Furthermore, the EDX mapping of the surface layer cross-sections showed that both P and Ca are evenly distributed within the coating layer. This further suggested that the PEO can be used to obtain coatings with potential propensity for osseointegration.

The XPS analysis supports our conclusion that the PEO with the chosen electrolyte components is a relatively "clean" process which gives rather predictable results (**Tab. 2**) Thus, P was found to exist only in the phosphate form (PO_4^{3-}), whereas Ca was found only in the form of calcium phosphate. Potassium, on the other hand, was only slightly incorporated into the oxide layers. Interestingly, nitrogen was also found in the PEO surfaces. The source of N was EDTA, which further emphasized potential advantage of the presence of this component in the batch electrolyte. In fact, nitrogen can be regarded as an important precondition for increased biocompatibility and ability to form tight junctions with living tissues. This process is not always straightforward and not yet thoroughly understood. Noteworthy, for instance, observation of the effects of locally applied Insulin-like Growth Factor-I on osseointegration with no positive responses after 2 weeks in both osteoporotic and normal rabbits [52].

The PEO layers showed favorable roughness of the implant surfaces. It is known that combination of a good surface roughness and mechanical properties of titanium could lead to successful dental implants [31]. However, the biological effects of titanium surfaces are not necessarily proportional to the degree of roughness in osteoblastic cultures or *in vivo* [53]. On the other hand, roughness could also lead to attachment of bacteria. The roughness of our PEO surfaces was generally high and was increasing with increased voltage/current (**Fig. 7**). Another aspect of biocompatibility is chemical resistance to corrosion, which was evaluated by the electrochemical corrosion assay (**Fig. 9, Tab. 4**). The PEO with bath electrolyte solution 2

Journal Pre-proof

showed superior corrosion resistance over the PEO treated Ti samples obtained in the electrolyte 1. This suggested that the corrosion resistance of the PEO surface layers can be enhanced by choosing optimal parameters for PEO treatment. The highest level of resistance was obtained with the Ti-2-400-150 sample. Long term corrosion resistance assay was also evaluated by prolonged (12 weeks) incubation in Ringer's solution (**Fig. 10**). Of all the samples tested, results show that the coatings in the sample Ti-2-450-150 is the least prone to corrosion among the treated samples and can therefore be chosen as a starting point for further development of the implant manufacturing. This corresponds to the data on the surface morphology revealed by SEM showing a robust oxide layer without cracks. In general, the coatings obtained with the bath no. 2 has a more anti-corrosion character than those treated in the bath no. 1. The higher release of Ti in the PEO treated samples in the Ringer's solution in comparison to untreated Ti (**Fig. 10**) can be explained by the fact, that under the conditions of the PEO process, during interaction of the sample material with the components of the electrolyte and formation of active chemical radicals at high temperature and pressure, the Ti is converted into ceramic-like material. It is rather inert, however is able to slowly react with the aggressive environment of the living tissues. The discrepancies between the electrochemical corrosion assay and the corrosion in Ringer's solution can partially be explained by the nature of the assay setups. Thus, in general the corrosion process under physiological conditions is mainly caused by chlorides. To this, the Ringer's solution is based on chlorides, which can mimic aggressive environments within the body. Overall, the sample Ti-2-450-150 showed the highest corrosion resistance. Importantly, this PEO protocol also showed favorable surface morphology without cracks revealed by the SEM. Taken together, the PEO protocol with bath electrolyte 2 can be suggested for further development of Ti dental implants.

Journal Pre-proof

The biocompatibility of the PEO surfaces was further tested in cell culture assay with rat osteoblasts (**Fig. 13**). All the PEO generated surfaces did not show any cytotoxicity. Then, the proliferation rate of the cells was dependent mainly on their ability to attach to the substrate. In general, the PEO surfaces showed favorable attachment to osteoblasts (**Fig. 14**). We concluded that the PEO conditions used to generate layer Ti-2-500-150 can be considered appropriate for further testing in order to obtain surfaces of implants with potential propensity for osseointegration of the surfaces of the Ti dental implants, and, possibly, higher implant stability in the long term. However, this also depends on the ability of implant surfaces to withstand attachment of bacterial cells and formation of biofilms. The bacterial adhesion assay showed that it indeed might be possible to find a balance between the ability of the bioactive surfaces to support growth of eukaryotic cells while inhibiting attachment and growth of bacteria (**Fig. 15**). However, the interplay between conditions to support cell attachment and proliferation, while preventing bacteria to attach and form biofilms, is dependent on delicate balance, and still requires further investigations.

While this project was in progress, a similar comprehensive study on the electrolyte composition and PEO conditions was published [20]. Our experimental data further corroborate the results described in that paper, and bring new dimensions into understanding of the PEO process. These studies will help to build a comprehensive mathematical model to generate bioactive surfaces using PEO and to establish protocols to manufacture bioactive surfaces on the next generation dental implants.

5. Conclusions

Oxides of Ti and other Ti compounds are formed during the PEO. It is possible to generate bioactive layers using Ca and P compounds on the surfaces of Ti implants. The electrolyte bath

solution number 2 promotes active crystallization of apatites after PEO processing of the Ti implants. The PEO layers can increase electrochemical corrosion resistance. The PEO can be potentially used for development of bioactive surfaces with increased support of eukaryotic cells while inhibiting attachment and growth of bacteria.

Acknowledgements

This work was supported by the National Center for Research and Development, Poland, under research Project No: POIR.01.01.02-00-0022/16. Cell culture and bacteriological experiment supported from Ministry of Education and Science of Ukraine grant (0119U100823). SK received support from Erasmus+ Jean Monnet grant 599989-EPP-1-2018-1-UA-EPPJMO-MODULE. The authors highly appreciate kind assistance of Dr. Sukhvinder Sandhu in language editing.

References

[1] D. Buser, T. von Arx, C. ten Bruggenkate, D. Weingart, Basic surgical principles with ITI implants, Clin. Oral Implants Res., 11 Suppl 1 (2000) 59-68. doi.org/10.1034/j.1600-0501.2000.011s1059.x.

[2] J. Darcey, D. Eldridge, Fifty Years of Dental Implant Development: a Continuous Evolution. Dent. Hist.: Lindsay Club News., 61 (2016) 75-92.

[3] M.S. Block, Dental Implants: The Last 100 Years, J. Oral Maxillofac. Surg., 76 (2018) 11-26. doi.org/10.1016/j.joms.2017.08.045

[4] A. Hafezeqoran, R. Koodaryan, Effect of Zirconia Dental Implant Surfaces on Bone Integration: A Systematic Review and Meta-Analysis, BioMed Res. Int., 2017 (2017) 9246721. doi.org/10.1155/2017/9246721

Journal Pre-proof

[5] K.I. Afrashtehfar, M. Del Fabbro, Clinical performance of zirconia implants: A meta-review, J. Prost. Dent., 123 (2020) 419-426. doi.org/ 10.1016/j.prosdent.2019.05.017

[6] T. Albrektsson, B. Chrcanovic, J. Molne, A. Wennerberg, Foreign body reactions, marginal bone loss and allergies in relation to titanium implants, Eur. J. Oral Implantol., 11 Suppl 1 (2018) S37-S46.

[7] A. Lugovskoy, S. Lugovskoy, Production of hydroxyapatite layers on the plasma electrolytically oxidized surface of titanium alloys, Mater. Sci. Eng. C, 43 (2014) 527-532. doi.org/10.1016/j.msec.2014.07.030

[8] H. Chouirfa, H. Bouloussa, V. Migonney, C. Falentin-Daudre, Review of titanium surface modification techniques and coatings for antibacterial applications, Acta Biomater., 83 (2019) 37-54. doi.org/10.1016/j.actbio.2018.10.036

[9] A. Insua, A. Monje, H.L. Wang, R.E. Miron, Basis of bone metabolism around dental implants during osseointegration and peri-implant bone loss, J. Biomed. Mater. Res. A, 105 (2017) 2075-2089. doi.org/10.1002/jbm.a.36060

[10] A. Gupta, S. Rathee, T. Suman, M. Ahire, S. Madhav, M.S. Chauhan, Nicotine, the predictor of success or failure of dental implants: A retrospective study, Contemp Clin Dent, 9 (2018) 597-600. doi.org/10.4103/ccd.ccd_597_18

[11] R. Smeets, B. Stadlinger, F. Schwarz, B. Beck-Broichsitter, O. Jung, C. Precht, F. Kloss, A. Grobe, M. Heiland, T. Ebker, BioMed Res. Int., Impact of Dental Implant Surface Modifications on Osseointegration, 2016 (2016) 6285620. doi.org/10.1155/2016/6285620

[12] M. Annunziata, L. Guida, The Effect of Titanium Surface Modifications on Dental Implant Osseointegration, Front. Oral Biol., 17 (2015) 62-77. doi.org/10.1159/000381694

Journal Pre-proof

[13] E. Matykina, R. Arrabal, P. Skeldon, G.E. Thompson, Transmission electron microscopy of coatings formed by plasma electrolytic oxidation of titanium, Acta Biomater., 5 (2009) 1356-1366. doi.org/10.1016/j.actbio.2008.10.007

[14] C.E. Tanase, M. Golozar, S.M. Best, R.A. Brooks, Cell response to plasma electrolytic oxidation surface-modified low-modulus β-type titanium alloys, Col. Surf. Biointerf., 176 (2019) 176-184. doi.org/10.1016/j.colsurfb.2018.12.064

[15] A. Kulkarni Aranya, S. Pushalkar, M. Zhao, R.Z. LeGeros, Y. Zhang, D. Saxena, Antibacterial and bioactive coatings on titanium implant surfaces, J. Biomed. Mater. Res. A, 105 (2017) 2218-2227. doi.org/10.1002/jbm.a.36081

[16] Q. Chen, W. Li, K. Ling, R. Yang, Investigation of Growth Mechanism of Plasma Electrolytic Oxidation Coating on Al-Ti Double-Layer Composite Plate, Materials, 12 (2019) 272. doi.org/10.3390/ma12020272

[17] B.L. Pereira, A.R. da Luz, C.M. Lepienski, I. Mazzaro, N.K. Kuromoto, Niobium treated by Plasma Electrolytic Oxidation with calcium and phosphorus electrolytes, J. Mech. Behav. Biomed. Mater., 77 (2018) 347-352. doi.org/10.1016/j.jmbbm.2017.08.010

[18] I. da Silva Vieira Marques, N.C. da Cruz, R. Landers, J.C.-C Yuan, M.F. Mesquita, C. Sukotjo, M.T. Mathew, V.A. Barao, Incorporation of Ca, P, and Si on bioactive coatings produced by plasma electrolytic oxidation: The role of electrolyte concentration and treatment duration, Biointerphases, 10 (2015) 041002. doi.org/10.1116/1.4932579

[19] M.P. Kamil, M. Kaseem, Y.G. Ko, Soft plasma electrolysis with complex ions for optimizing electrochemical performance, Sci. Rep., 7 (2017) 44458. doi.org/10.1038/srep44458

Journal Pre-proof

[20] A. Santos-Coquillat, M. Mohedano, E. Martinez-Campos, R. Arrabal, A. Pardo, E. Matykina, Bioactive multi-elemental PEO-coatings on titanium for dental implant applications, Mater. Sci. Eng. C, 97 (2019) 738-752. doi.org/10.1016/j.msec.2018.12.097

[21] K. Leśniak-Ziółkowska, A. Kazek-Kęsik, Krzysztof Rokosz, S. Raaen, A. Stolarczyk, M. Krok-Borkowicz, E. Pamuła, M. Gołda-Cępa, M. Brzychczy-Włoch, W. Simka, Electrochemical modification of the Ti-15Mo alloy surface in solutions containing ZnO and $Zn_3(PO_4)_2$ particles, Mater. Sci. Eng. C, 115 (2020) 111098. doi.org/10.1016/j.msec.2020.111098

[22] A. Kazek-Kęsik, I. Kalemba-Rec, W. Simka, Anodization of a Medical-Grade Ti-6Al-7Nb Alloy in a $Ca(H_2PO_2)_2$-Hydroxyapatite Suspension, Materials, 12 (2019) 3002. 10.3390/ma12183002.

[23] C.T. Rueden, J. Schindelin, M.C. Hiner, B.E. DeZonia, A.E. Walter, E.T. Arena, K.W. Eliceiri, ImageJ2: ImageJ for the next generation of scientific image data, BMC Bioinformatics, 18 (2017) 529. doi.org/10.1186/s12859-017-1934-z

[24] M. Basiaga, W. Kajzer, W. Walke, A. Kajzer, M. Kaczmarek, Evaluation of physicochemical properties of surface modified Ti6Al4V and Ti6Al7Nb alloys used for orthopedic implants, Mater. Sci. Eng. C, 68 (2016) 851-860. doi.org/10.1016/j.msec.2016.07.042

[25] V. Korniienko, O. Oleshko, Y. Husak, V. Deineka, V. Holubnycha, O. Mishchenko, A. Kazek-Kęsik, A. Jakóbik-Kolon, R. Pshenychnyi, K. Leśniak-Ziółkowska, O. Kalinkevich, A. Kalinkevich, M. Pisarek, W. Simka, M. Pogorielov, Formation of a Bacteriostatic Surface on ZrNb Alloy via Anodization in a Solution Containing Cu Nanoparticles, Materials, 13 (2020) 3913. doi.org/10.3390/ma13183913

[26] T. Kokubo, Apatite formation on surfaces of ceramics, metals and polymers in body environment, Acta Mater., 46 (1998) 2519-2527. doi.org/10.1016/S1359-6454(98)80036-0

Journal Pre-proof

[27] G. Mortazavi, J. Jiang, E.I. Meletis, Investigation of the plasma electrolytic oxidation mechanism of titanium, Appl. Surf. Sci., 488 (2019) 370-382. doi.org/10.1016/j.apsusc.2019.05.250

[28] M. Pisarek, A. Roguska, M. Andrzejczuk, L. Marcon, S. Szunerits, M. Lewandowska, M. Janik-Czachor, Effect of two-step functionalization of Ti by chemical processes on protein adsorption, Appl. Surf. Sci., 257 (2011) 8196-8204. doi.org/10.1016/j.apsusc.2011.03.120

[29] M. Sowa, M. Parafiniuk, C.M.S. Mouzêlo, A. Kazek-Kęsik, I.S. Zhidkov, A.I. Kukharenko, S.O. Cholakh, E.Z. Kurmaev, W. Simka, DC plasma electrolytic oxidation treatment of gum metal for dental implants, Electrochim. Acta, 302 (2019) 10-20. doi.org/10.1016/j.electacta.2019.02.024

[30] J. Chastain, J.F. Moulder, Physical Electronics Inc., Eden Prairie, Minnesota, USA, 1995.

[31] A. Jemat, M.J. Ghazali, M. Razali, Y. Otsuka, Surface Modifications and Their Effects on Titanium Dental Implants, BioMed Res. Int., 2015 (2015) 791725. doi.org/10.1155/2015/791725

[32] M. Mohedano, E. Matykina, R. Arrabal, A. Pardo, M.C. Merino, Metal release from ceramic coatings for dental implants, Dent. Mater., 30 (2014) e28-40. doi.org/10.1016/j.dental.2013.12.011

[33] I.D. Marques, V.A. Barao, N.C. da Cruz, J.C. Yuan, M.F. Mesquita, A.P. Ricomini-Filho, C. Sukotjo, M.T. Mathew, Electrochemical behavior of bioactive coatings on cp-Ti surface for dental application, Corr. Sci., 100 (2015) 133-146. doi.org/10.1016/j.corsci.2015.07.019

[34] M.A. Khan, R.L. Williams, D.F. Williams, In-vitro corrosion and wear of titanium alloys in the biological environment, Biomaterials, 17 (1996) 2117-2126. doi.org/10.1016/0142-9612(96)00029-4

Journal Pre-proof

[35] V.Z. de Souza, R. Manfro, J.C. Joly, C.N. Elias, D.C. Peruzzo, M.H. Napimoga, E.F. Martinez, Viability and collagen secretion by fibroblasts on titanium surfaces with different acid-etching protocols, Int. J. Implant Dent., 5 (2019) 41. doi.org/10.1186/s40729-019-0192-4

[36] C.J. Chung, R.T. Su, H.J. Chu, H.T. Chen, H.K. Tsou, J.L. He, Plasma electrolytic oxidation of titanium and improvement in osseointegration, J. Biomed. Mater. Res. B Appl. Biomater., 101 (2013) 1023-1030. doi.org/10.1002/jbm.b.32912

[37] L. Polo-Corrales, M. Latorre-Esteves, J.E. Ramirez-Vick, Scaffold Design for Bone Regeneration, J. Nanosci. Nanotechn., 14 (2014) 15-56. doi.org/10.1166/jnn.2014.9127

[38] A.R. Rafieerad, M.R. Ashra, R. Mahmoodian, A.R. Bushroa, Surface characterization and corrosion behavior of calcium phosphate-base composite layer on titanium and its alloys via plasma electrolytic oxidation: A review paper, Mater. Sci. Eng. C, 57 (2015) 397-413. doi.org/10.1016/j.msec.2015.07.058

[39] M.R. Etminanfar, J. Khalil-Allafi, A. Montaseri, R. Vatankhah-Barenji, Endothelialization and the bioactivity of Ca-P coatings of different Ca/P stoichiometry electrodeposited on the Nitinol superelastic alloy, Mater. Sci. Eng. C, 2 (2016) 28-35. doi.org/10.1016/j.msec.2016.01.036

[40] S. Best, B. Sim, M. Kayser, S. Downes, The dependence of osteoblastic response on variations in the chemical composition and physical properties of hydroxyapatite, J. Mater. Sci. Mater. Med., 8 (1997) 97-103. doi.org/10.1023/A:1018558816871

[41] F. Monchau, P. Hivart, B. Genestie, F. Chai, M. Descamps, H.F. Hildebrand, Calcite as a bone substitute. Comparison with hydroxyapatite and tricalcium phosphate with regard to the osteoblastic activity, Mater. Sci. Eng. C, 33 (2013) 490-498. doi.org/10.1016/j.msec.2012.09.019

Journal Pre-proof

[42] Q.M. Zhao, X.K. Li, S. Guo, N. Wang, W.W. Liu, L. Shi, Z. Guo, Osteogenic activity of a titanium surface modified with silicon-doped titanium dioxide, Mater. Sci. Eng. C, 110 (2020) 110682. doi.org/10.1016/j.msec.2020.110682

[43] J. Li, X. Cui, G.J. Hooper, K.S. Lim, T.B.F. Woodfield, Rational design, bio-functionalization and biological performance of hybrid additive manufactured titanium implants for orthopaedic applications: A review, J. Mech. Behav. Biomed. Mater., 105 (2020) 103671. doi.org/10.1016/j.jmbbm.2020.103671

[44] C. Aparicio, M.-P. Ginebra, Biomineralization and Biomaterials, Fundamentals and Applications, Woodhead Publishing, 2016, pp. 482.

[45] N. Gui, W. Xu, A.N. Abraham, D.E. Myers, E.L.H. Mayes, K. Xia, R. Shukla, M. Qian, A comparative study of the effect of submicron porous and smooth ultrafine- grained Ti- 20Mo surfaces on osteoblast responses, J. Biomed. Mater. Res. A, 106 (2018) 2020-2033. doi.org/10.1002/jbm.a.36402

[46] J. Zhou, L. Zhao, Hypoxia-mimicking Co doped TiO_2 microporous coating on titanium with enhanced angiogenic and osteogenic activities, Acta Biomater., 43 (2016) 358-368. doi.org/10.1016/j.actbio.2016.07.045

[47] Q. Wang, Y.B. Hong, M.D. Huang, Q.M. Wang, W. Teng, Constructing self-adhesive and robust functional films on titanium resistant to mechanical damage during dental implanting, Mater. Sci. Eng. C, 110 (2020) 110688. doi.org/10.1016/j.msec.2020.110688

[48] R.F. do Prado, G.C. Esteves, E.L.S. Santos, D.A.G. Bueno, C.A.A. Cairo, L.G.O. Vasconcellos, R.S. Sagnori, F.B.P. Tessarin, F.E. Oliveira, L.D. Oliveira, M.F.L. Villaca-Carvalho, V.A.R. Henriques, Y.R. Carvalho, L.M.R. De Vasconcellos, n vitro and in vivo

Journal Pre-proof

biological performance of porous Ti alloys prepared by powder metallurgy, PLOS ONE, 13 (2018) e0196169. doi.org/10.1371/journal.pone.0196169

[49] S. Prasadh, R.C.W. Wong, Unraveling the mechanical strength of biomaterials used as a bone scaffold in oral and maxillofacial defects, Oral Sci. Inter., 15 (2018) 48-55. doi.org/10.1016/S1348-8643(18)30005-3

[50] S. Prasadh, S. Suresh, K.L. Hong, A. Bhargav, V. Rosa, R.C.W. Wong, Biomechanics of alloplastic mandible reconstruction using biomaterials: The effect of implant design on stress concentration influences choice of material, J. Mech. Behav. Biomed. Mater., 103 (2020) 103548. doi.org/ 10.1016/j.jmbbm.2019.103548

[51] O. Mishchenko, O. Ovchynnykov, O. Kapustian, M. Pogorielov, New Zr-Ti-Nb Alloy for Medical Application: Development, Chemical and Mechanical Properties, and Biocompatibility, Materials, 13 (2020) 1306. doi.org/10.3390/ma13061306

[52] J. Lopez-Quiles, A. Forteza-Lopez, M. Montiel, C. Clemente, J.A. Fernandez-Tresguerres, I. Fernandez-Tresguerres, Effects of locally applied Insulin-like Growth Factor-I on osseointegration, Med. Oral Patol. Oral Cir. Bucal., 24 (2019) e652-e658. doi.org/ 10.4317/medoral.22973

[53] J. Saruta, N. Sato, M. Ishijima, T. Okubo, M. Hirota, T. Ogawa, Disproportionate Effect of Sub-Micron Topography on Osteoconductive Capability of Titanium, Int. J. Mol. Sci., 20 (2019) 4027. doi.org/ 10.3390/ijms20164027

Journal Pre-proof

Figure 1. Representative SEM images of the selected samples after PEO process (the complete set of SEM images with electrolytes 1, 2, 3 and 4 is presented in the **Supplement Fig. 2**). **A**, sample Ti-1-450-150; **B**, sample Ti-1-500-150; **C**, sample Ti-2-400-100; **D**, sample Ti-2-400-150; **E**, sample Ti-2-450-100; **F**, sample Ti-2-500-150. Magnification x2000, scale bars = 30 μm

Figure 2. Distribution of the pores size in Ti samples after PEO process. **A**, sample Ti-1-450-150; **B**, sample Ti-1-500-150; **C**, sample Ti-2-400-100; **D**, sample Ti-2-400-150; **E**, sample Ti-2-450-100; **F**, sample Ti-2-500-150. Magnification x2000, scale bars = 30 μm

Figure 3. Representative EDX spectra of the selected samples after PEO process. **A**, sample Ti-1-450-150; **B**, sample Ti-1-500-150; **C**, sample Ti-2-400-100; **D**, sample Ti-2-400-150; **E**, sample Ti-2-450-100; **F**, sample Ti-2-500-150. Magnification x2000, scale bars = 30 μm

Figure 4. An exemplary SEM image and an EDX mapping of Ti-2-500-250 sample cross-section, scale bar = 10 μm

Figure 5. Raman spectra of samples with different phosphate contents. Comparison of phosphate content was done based on phosphate vibration intensity 1006 cm^{-1} to TiO_2 144 cm^{-1} for the selected PEO surfaces

Journal Pre-proof

Figure 6. XRD plots showing data for the Ti-1-450-150, Ti-1-500-150, Ti-2-400-100 Ti-2-400-150, and Ti-2-500-150 samples

Figure 7. Roughness of selected surfaces (shown in arbitrary units) and contact angle (measured with a drop of water)

Figure 8. Adhesion of the oxide layer to the Ti substrate demonstrated by the scratch test. **A**, representative pictures of the scratches in the surface of the oxide layers; **B**, quantification of the results

Figure 9. Bode plots showing **A**, impedance magnitude ($|Z|$); **B**, negative phase angle ($-\Phi$) relationships with frequency for the non-treated titanium sample and the PEO treated samples. × signify the points calculated from the fitting of the experimental data to the $R_s(Q_{bar}R_{bar})$ model for the non-treated titanium, and the EEC depicted in **C** for the PEO-treated samples; **D**, PDP curves recorded for the non-treated titanium samples and after the PEO treatment as indicated

Figure 10. Release of specific elements after prolonged incubation in Ringer's solution for 12 weeks. Analytical ICP-OES assay was done every 2 weeks. **A**, release of Ti ions; **B**, release of P ions. The data showed statistical significance at $p<0.05$

Figure 11. Representative SEM images of the surface of the Ti-2-400-150 sample after the bioactivity test in SBF solution, scale bars = 100 μm

Figure 12. The EDX spectra of samples Ti-2-400-100 (A) and Ti-2-450-150 (B) after the bioactivity test in SBF solution

Journal Pre-proof

Figure 13. Cytotoxicity / cell viability assay. Statistical significance was evaluated in comparison to the reference of each time point (p values after by two-tailed two sample equal variance test)

Figure 14. Scanning electron microscopy of osteoblast distribution over the experimental surfaces on day 7 after cell seeding, scale bars = 500 µm

Figure 15. Bacterial adhesion. The amount of bacteria adhered to the surfaces of the samples at different time points of incubation. The data are shown as means with SD values. Asterisks indicate p values where ** - p<0.01; *** - p<0.001 (one-way ANOVA)

Table 1. Listing of the electrolyte components (concentrations in Mol L^{-1})

Electrolyte	**EDTA**	**KH_2PO_4**	**$Ca(OH)_2$**	**$Ca(HCOO)_2$**	**pH**
1	0.017	0.006	0.023		3.73
2	0.034	0.012	0.046		3.82
3	0.017	0.006		0.013	3.18
4	0.034	0.012		0.026	3.24

Table 2. Quantification of the XPS analysis of the PEO surfaces

Element	Si	P	C	K	Ca	N	Ti	O	**Ca/P ratio**
Ti-1-450-150	0.8	7.8	39.9	0	1.4	1.4	9.9	38.9	**0.18**
Ti-2-400-100	0.3	13.1	13.8	0.1	2.6	2.2	12.1	55.8	**0.20**

Ti-2-500-150	0.6	13.7	15.8	0.2	3.6	2.2	9.9	54	**0.26**

Table 3. Comparison of phosphate content based on phosphate vibration intensity 1006 cm^{-1} to TiO_2 144 cm^{-1}

Sample	I_{1006}/I_{144}
Ti-1-450-150	0.00371
Ti-1-500-150	0.00302
Ti-2-400-100	0.01482
Ti-2-400-150	0.01237
Ti-2-450-100	0.00561
Ti-2-500-150	0.01497

Table 4. Parameters obtained from the fitting of the EIS data to the $R_s(Q_{bar}R_{bar})$ model in the case of the bare Ti sample, and the EEC shown in Fig. 7C for the PEO-treated titanium samples

Sample	bare Ti	Ti-1-450-150	Ti-1-500-150	Ti-2-400-150	Ti-2-500-150
R_s (Ω cm^2)	20.6	22.3	23.9	25.1	24.5
Q_{coat} (s^n $M\Omega^{-1}$ cm^{-2})	–	1.43	1.56	0.186	0.159
n_{coat} (–)	–	0.77	0.77	0.87	0.89
R_{po} ($k\Omega$ cm^2)	–	5.01	7.74	47.5	66.0
δ ($k\Omega$ $s^{½}$)	–	13.0	16.0	71.4	63.8
Q_{bar} (s^n $M\Omega^{-1}$ cm^{-2})	24.0	34.5	25.6	14.9	24.5
n_{bar} (–)	0.93	0.91	0.90	0.97	1.00
R_{bar} ($M\Omega$ cm^2)	1.73	9.37	6.39	11.3	6.69
χ^2 (–)	$< 8.46 \cdot 10^{-4}$	$< 2.08 \cdot 10^{-4}$	$< 2.66 \cdot 10^{-4}$	$< 1.04 \cdot 10^{-4}$	$< 1.26 \cdot 10^{-3}$

Journal Pre-proof

Table 5. Corrosion data extracted from the polarization experiments performed in the short-range (LPR) and long-range (PDP)

Sample	bare Ti	Ti-1-450-150	Ti-1-500-150	Ti-2-400-150	Ti-2-500-150
E_{OC} (mV *vs*. SCE)	−39.7	238.8	276.9	313.1	319.3
$E_{cor,LPR}$ (mV *vs*. SCE)	−30.3	214.6	288.3	308.0	321.1
$E_{cor,PDP}$ (mV *vs*. SCE)	−77.4	104.4	162.8	184.4	198.0
R_p (MΩ cm^2)	6.91	23.4	26.8	61.9	26.1
i_{pas} (nA cm^{-2})	407	14.2	9.17	3.91	6.91

Journal Pre-proof

Journal Pre-proof

Authors statement

Sergiy Kyrylenko: Conceptualization, Validation, Data curation, Writing - original draft, Writing - review &editing. **Fiona Warchoł:** Methodology, Validation, Formal analysis, Investigation. **Oleksandr Oleshko:** Methodology, Validation, Formal analysis, Investigation. **Eugenia Husak:** Methodology, Validation, Formal analysis, Investigation. **Alicja Kazek-Kęsik:** Methodology, Validation, Formal analysis, Investigation. **Viktoriia Korniienko:** Methodology, Validation, Formal analysis, Investigation. **Volodymyr Deineka:** Methodology, Validation, Formal analysis, Investigation. **Maciej Sowa:** Methodology, Validation, Formal analysis, Investigation. **Artur Maciej:** Methodology, Validation, Formal analysis, Investigation. **Joanna Michalska:** Methodology, Validation, Formal analysis, Investigation. **Agata Jakóbik-Kolon:** Methodology, Validation, Formal analysis, Investigation. **Izabela Matuła:** Methodology, Validation, Formal analysis, Investigation. **Marcin Basiaga:** Methodology, Validation, Formal analysis, Investigation. **Viktoriia Humbnycha:** Methodology, Validation, Formal analysis, Investigation. **Agnieszka Stolarczyk:** Methodology, Validation, Formal analysis, Investigation. **Marcin Pisarek:** Methodology, Validation, Formal analysis, Investigation. **Oleg Mishchenko:** Conceptualization, Formal analysis, Validation, Data Curation. **Maksym Pogorielov:** Conceptualization, Formal analysis, Validation, Data Curation, Writing - Original Draft, Writing - Review & Editing, Supervision. **Wojciech Simka:** Conceptualization, Formal analysis, Validation, Data Curation, Writing - Original Draft, Writing - Review & Editing, Supervision, Project administration.

Conflict of interest

O.M., M.P., W.S. are employed by Nano Prime. The authors declare that they have no competing financial interests or personal relationships that could have influenced the results reported in this paper.

Journal Pre-proof

Journal Pre-proof

Highlights

- Ceramic coatings on titanium dental implants were obtained via plasma electrolytic oxidation (PEO) with calcium and phosphate ions.
- Ethylenediamine tetraacetic acid greatly enhanced efficiency of deposition of calcium and phosphorus into the PEO generated surface layers.
- PEO surface layers induce crystallization of apatites upon exposure to body-like environment in simulated body fluids.
- PEO can be used for formation of bioactive surfaces which support attachment and proliferation of eukaryotic cells while inhibiting attachment and growth of bacteria.

Journal Pre-proof

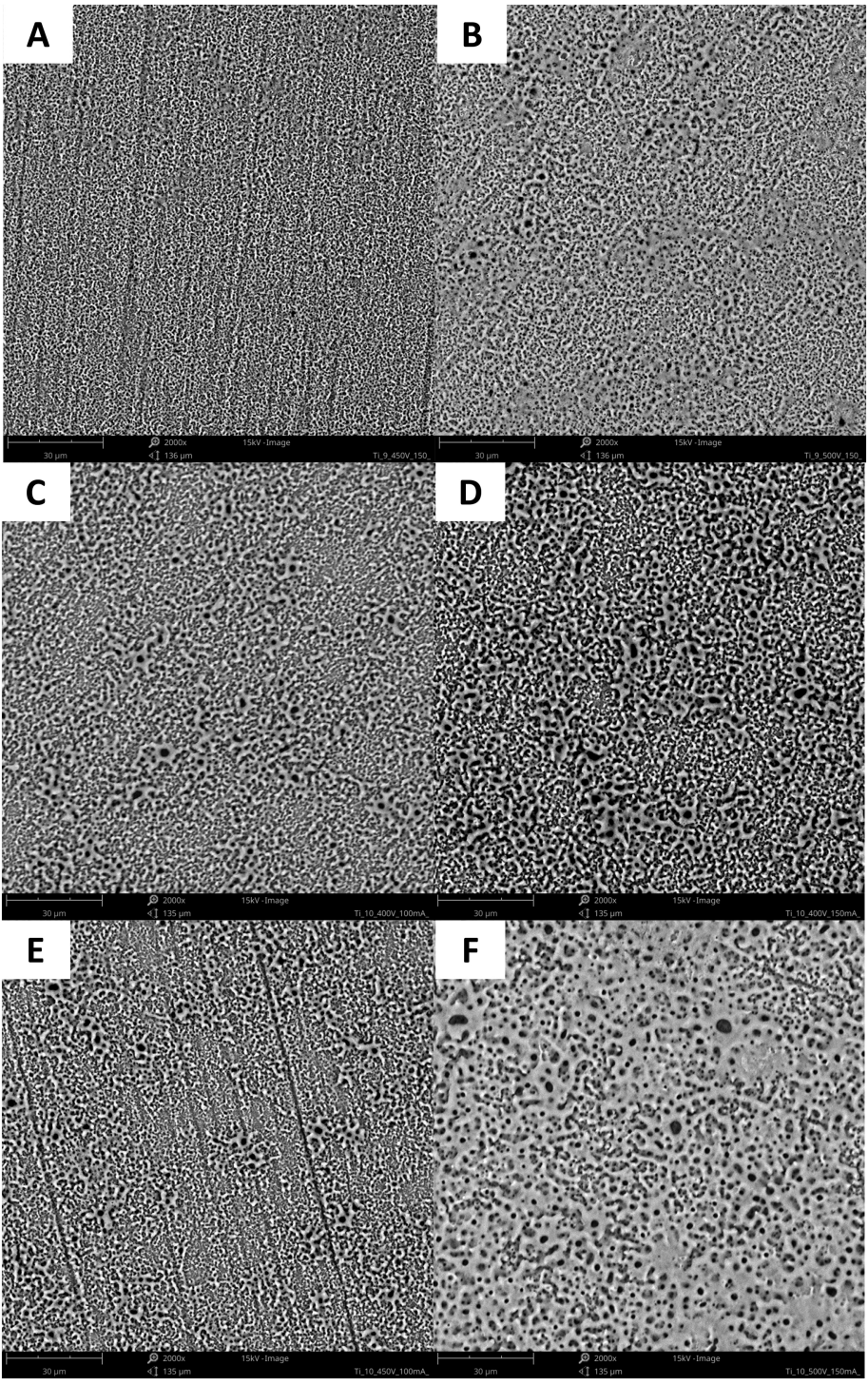
A
30 µm
2000x
15kV - Image
136 µm
Ti_9_450V_150
B
30 µm
2000x
15kV - Image
136 µm
Ti_9_500V_150
C
30 µm
2000x
15kV - Image
135 µm
Ti_10_400V_100mA_
D
30 µm
2000x
15kV - Image
135 µm
Ti_10_400V_150mA_
E
30 µm
2000x
15kV - Image
135 µm
Ti_10_450V_100mA_
F
30 µm
2000x
15kV - Image
135 µm
Ti_10_500V_150mA_

Figure 1

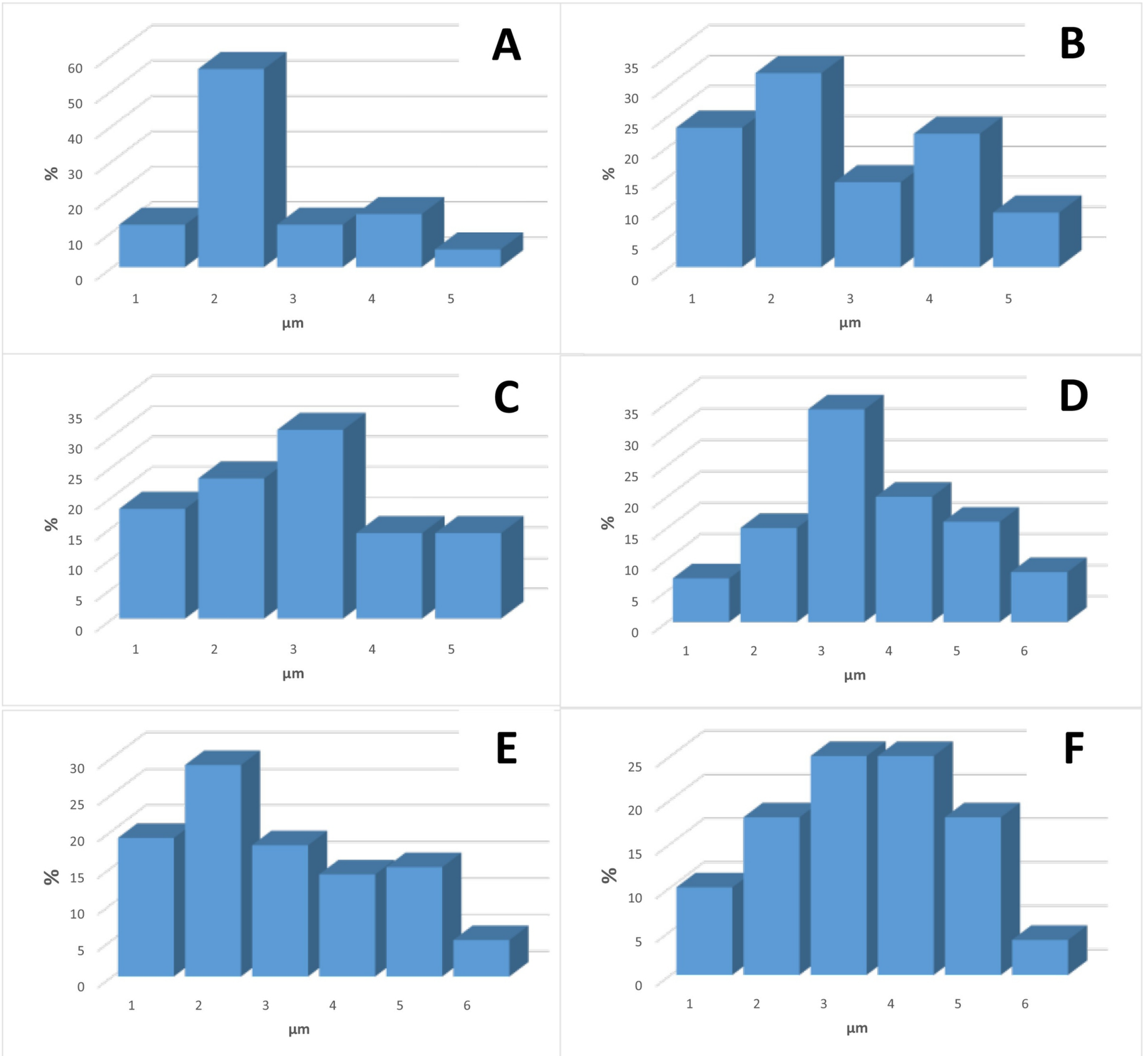
A
%
60
50
40
30
20
10
0
1
2
3
4
5
µm
B
%
35
30
25
20
15
10
5
0
1
2
3
4
5
µm
C
%
35
30
25
20
15
10
5
0
1
2
3
4
5
µm
D
%
35
30
25
20
15
10
5
0
1
2
3
4
5
6
µm
E
%
30
25
20
15
10
5
0
1
2
3
4
5
6
µm
F
%
25
20
15
10
5
0
1
2
3
4
5
6
µm

Figure 2

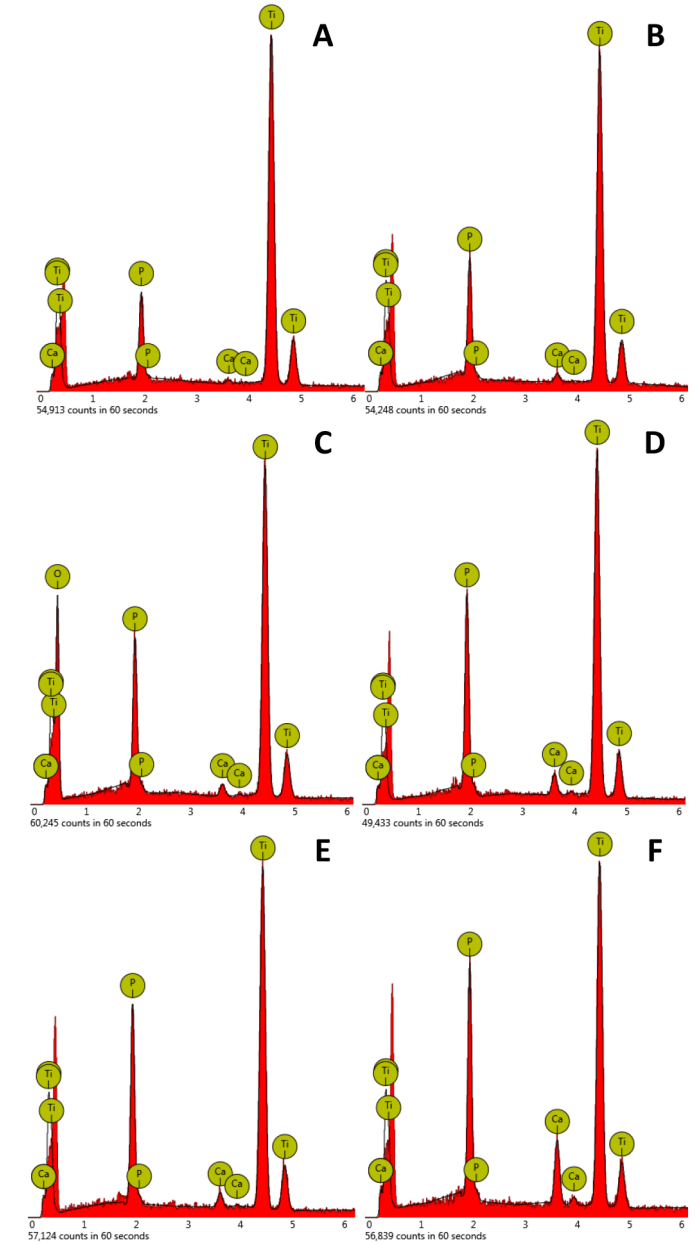
A
B
C
D
E
F
Ti
P
Ca
O
0 1 2 3 4 5 6
54,913 counts in 60 seconds
54,248 counts in 60 seconds
60,245 counts in 60 seconds
49,433 counts in 60 seconds
57,124 counts in 60 seconds
56,839 counts in 60 seconds

Figure 3

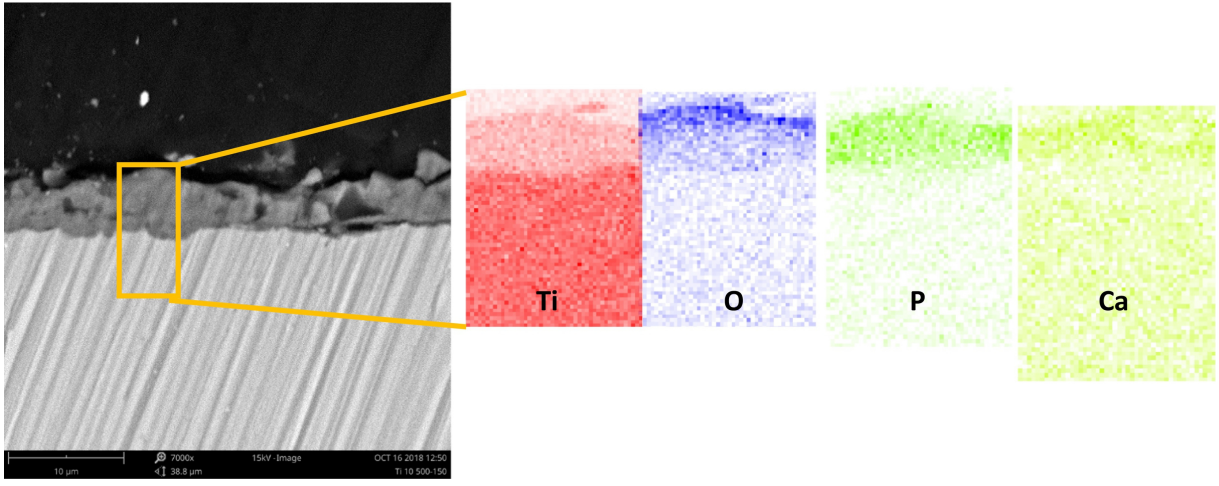
10 µm
7000x
38.8 µm
15kV -Image
OCT 16 2018 12:50
Ti 10 500-150
Ti
O
P
Ca

Figure 4

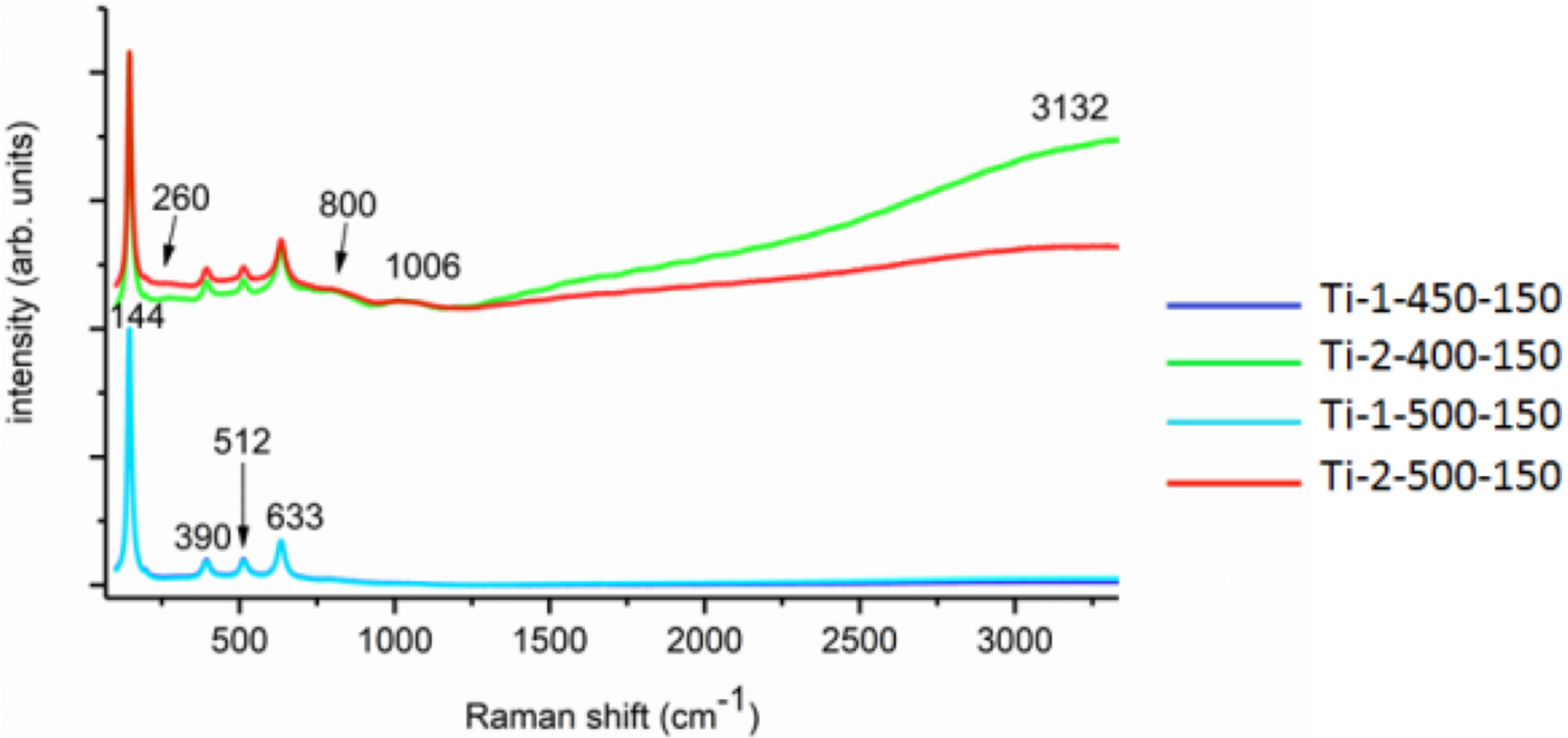
intensity (arb. units)
3132
260
800
1006
144
512
390
633
500
1000
1500
2000
2500
3000
Raman shift (cm-1)
Ti-1-450-150
Ti-2-400-150
Ti-1-500-150
Ti-2-500-150

Figure 5

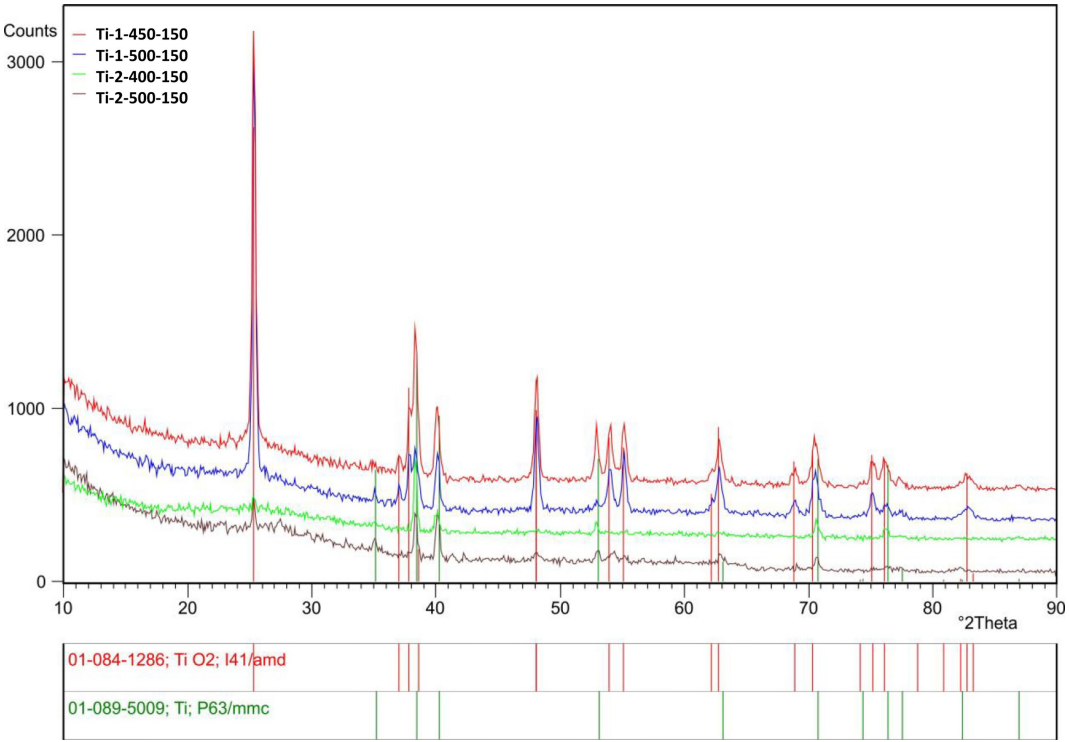
Counts
Ti-1-450-150
Ti-1-500-150
Ti-2-400-150
Ti-2-500-150
3000
2000
1000
0
10
20
30
40
50
60
70
80
90
°2Theta
01-084-1286; Ti O2; I41/amd
01-089-5009; Ti; P63/mmc

Figure 6

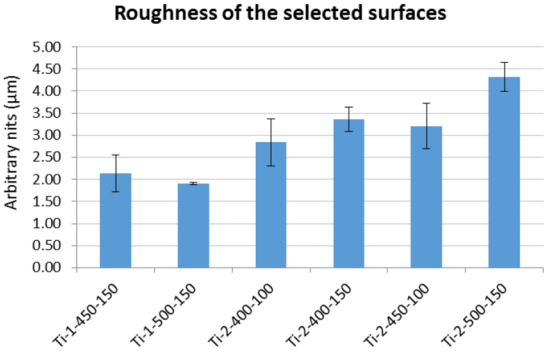
Roughness of the selected surfaces
Arbitrary nits (µm)
5.00
4.50
4.00
3.50
3.00
2.50
2.00
1.50
1.00
0.50
0.00
Ti-1-450-150
Ti-1-500-150
Ti-2-400-100
Ti-2-400-150
Ti-2-450-100
Ti-2-500-150

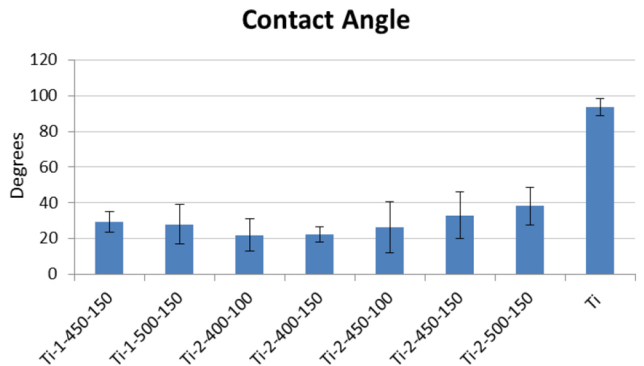
Contact Angle
Degrees
120
100
80
60
40
20
0
Ti-1-450-150
Ti-1-500-150
Ti-2-400-100
Ti-2-400-150
Ti-2-450-100
Ti-2-450-150
Ti-2-500-150
Ti

Figure 7

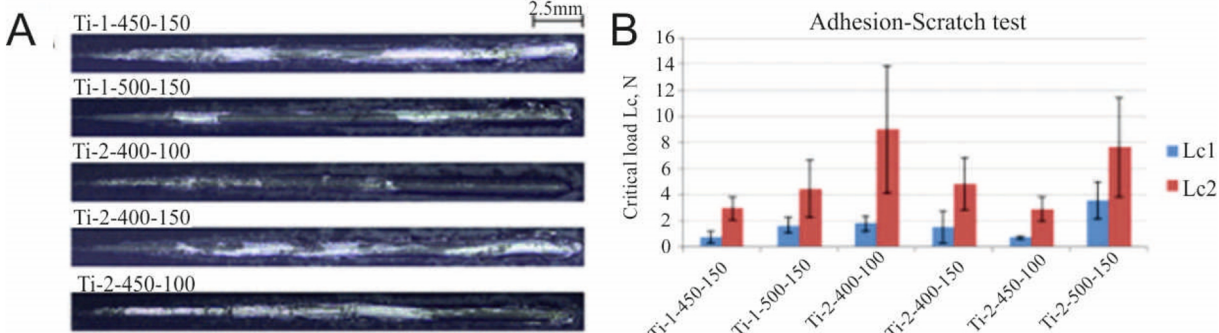
A
2.5mm
Ti-1-450-150
Ti-1-500-150
Ti-2-400-100
Ti-2-400-150
Ti-2-450-100
B
Adhesion-Scratch test
Critical load Lc, N
16
14
12
10
8
6
4
2
0
Lc1
Lc2
Ti-1-450-150
Ti-1-500-150
Ti-2-400-100
Ti-2-400-150
Ti-2-450-100
Ti-2-500-150

Figure 8

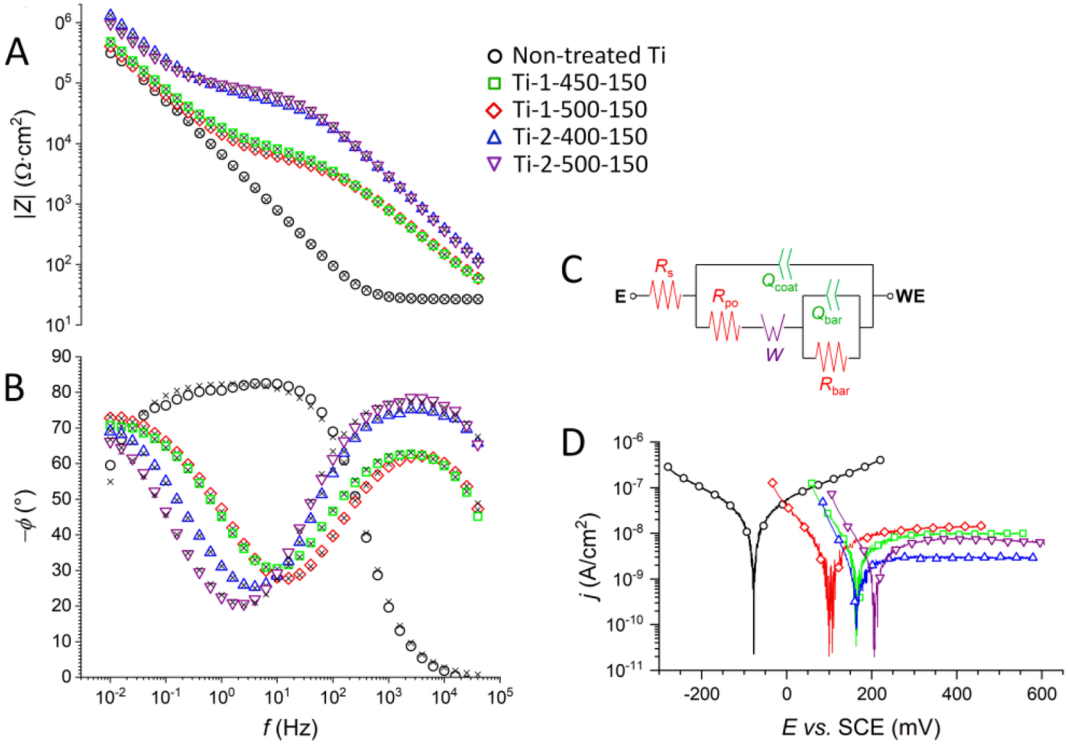
A
Non-treated Ti
Ti-1-450-150
Ti-1-500-150
Ti-2-400-150
Ti-2-500-150
|Z| (Ω·cm²)
B
−ϕ (°)
f (Hz)
C
E
WE
Rs
Rpo
Qcoat
Qbar
W
Rbar
D
j (A/cm²)
E vs. SCE (mV)

Figure 9

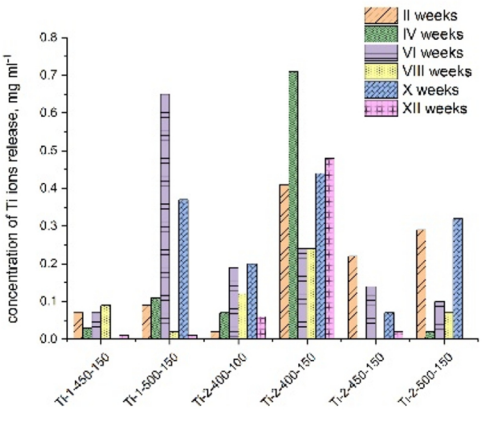
II weeks
IV weeks
VI weeks
VIII weeks
X weeks
XII weeks
concentration of Ti ions release, mg ml-1
0.0
0.1
0.2
0.3
0.4
0.5
0.6
0.7
0.8
Ti-1-450-150
Ti-1-500-150
Ti-2-400-100
Ti-2-400-150
Ti-2-450-150
Ti-2-500-150

A

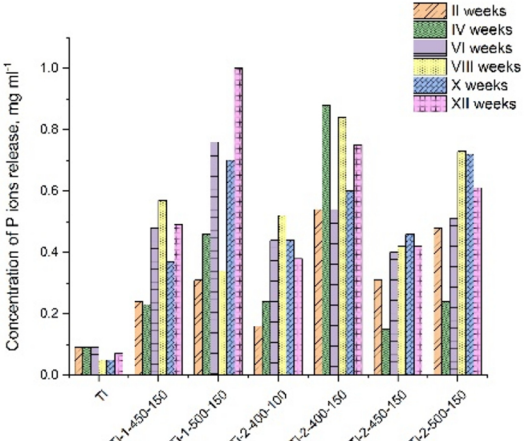
II weeks
IV weeks
VI weeks
VIII weeks
X weeks
XII weeks
Concentration of P ions release, mg ml-1
0.0
0.2
0.4
0.6
0.8
1.0
Ti
Ti-1-450-150
Ti-1-500-150
Ti-2-400-100
Ti-2-400-150
Ti-2-450-150
Ti-2-500-150

B

Figure 10

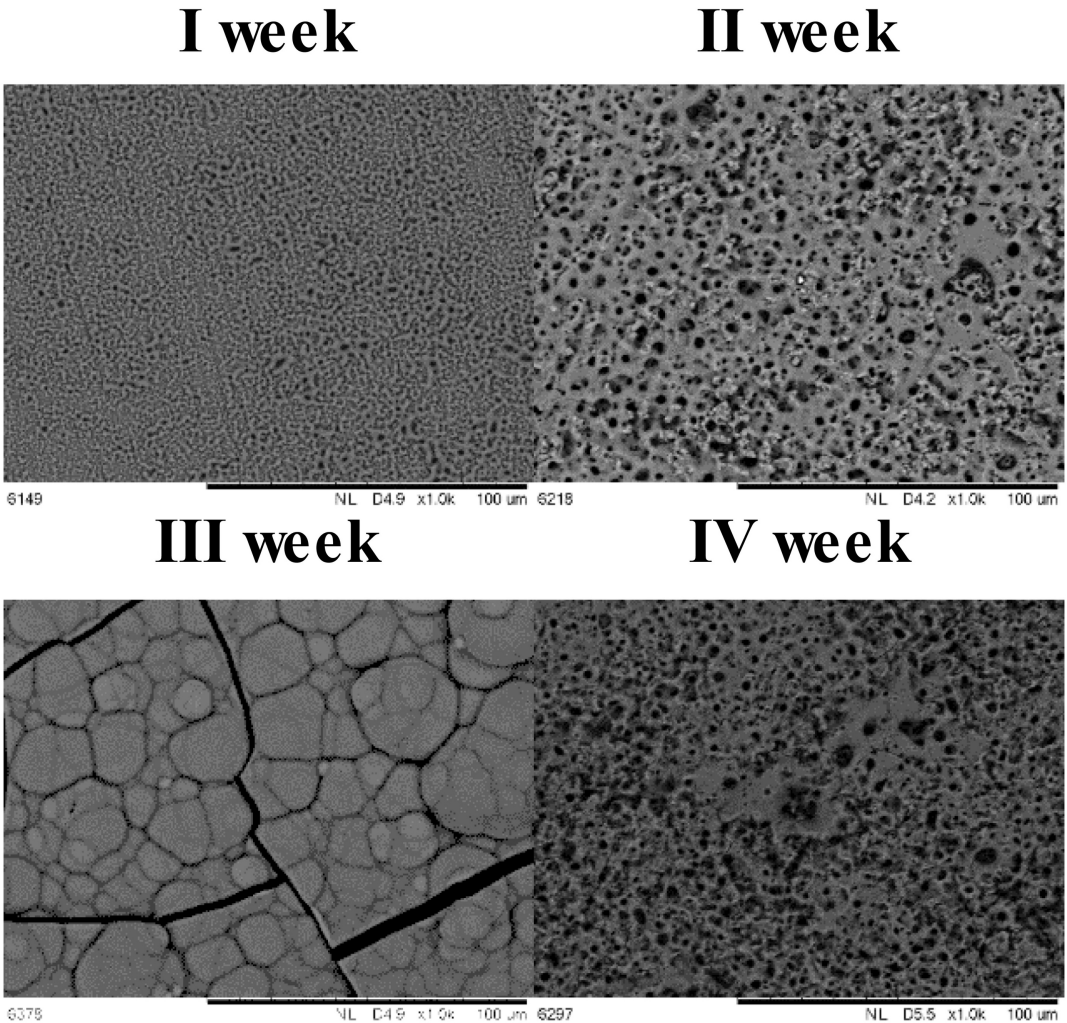
I week
II week
6149
NL D4.9 x1.0k 100 um
6218
NL D4.2 x1.0k 100 um
III week
IV week
6378
NL D4.9 x1.0k 100 um
6297
NL D5.5 x1.0k 100 um

Figure 11

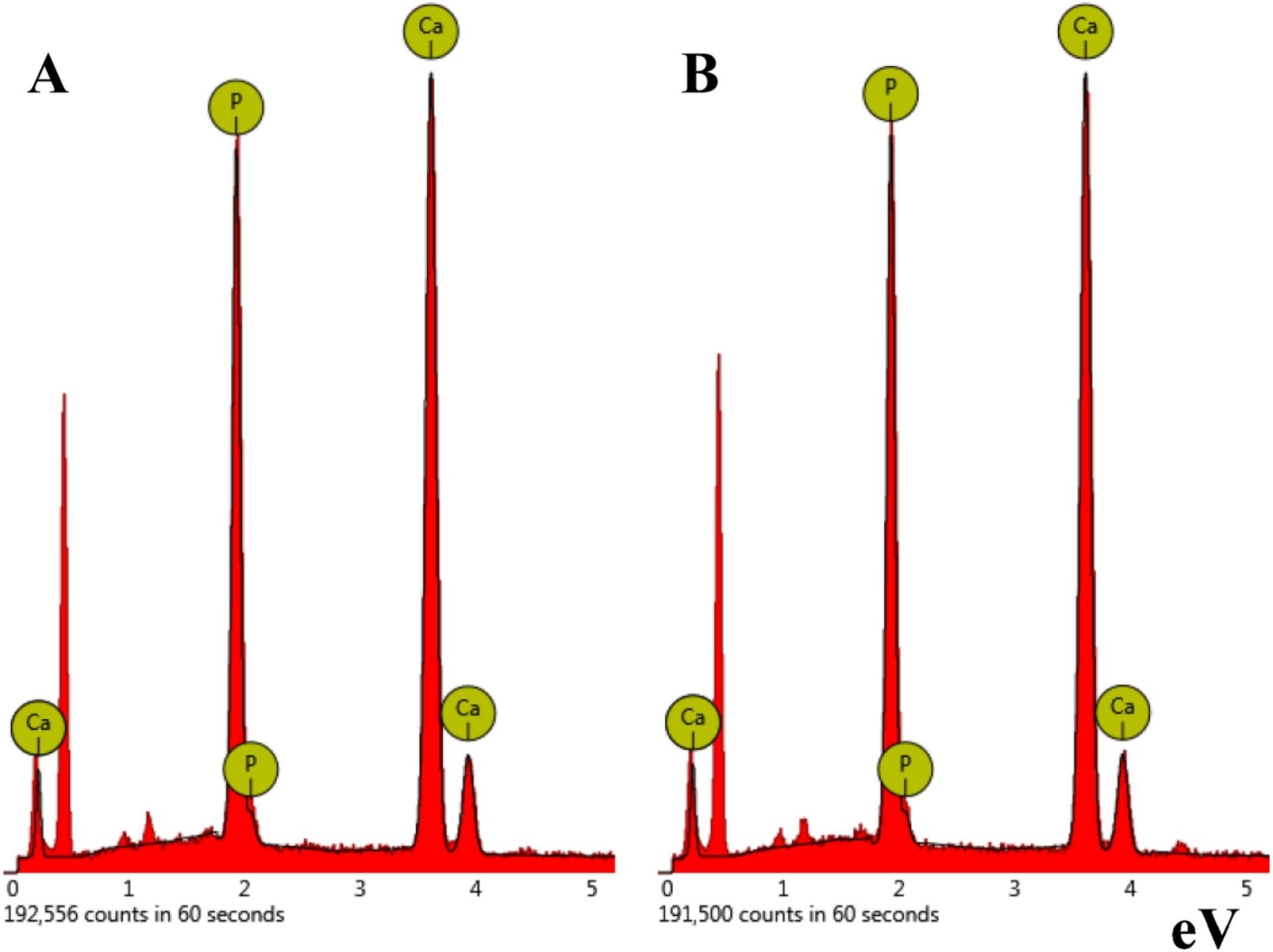
A
Ca
P
Ca
P
Ca
0
1
2
3
4
5
192,556 counts in 60 seconds
B
Ca
P
Ca
Ca
P
Ca
0
1
2
3
4
5
191,500 counts in 60 seconds
eV

Figure 12

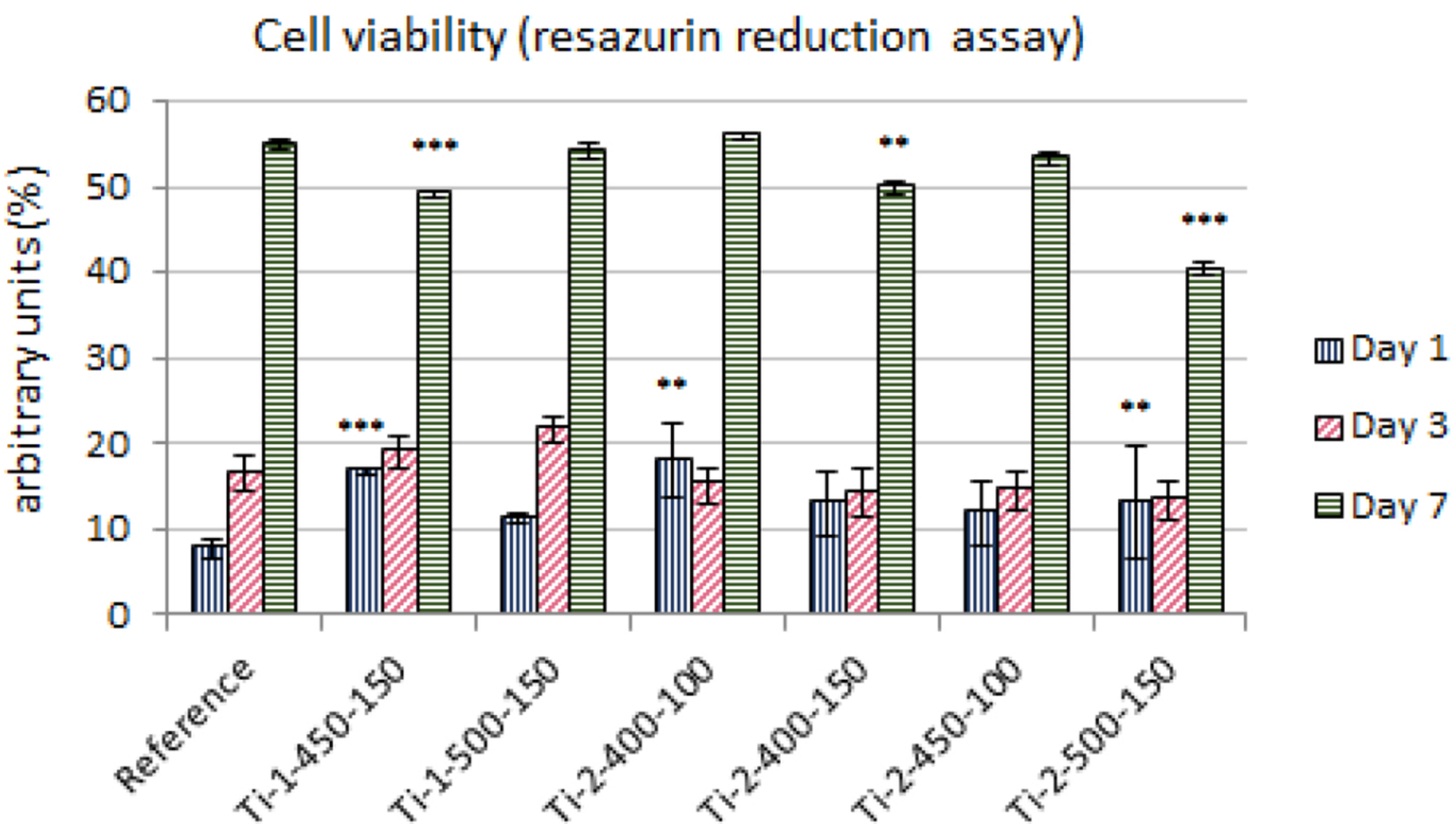
Cell viability (resazurin reduction assay)
arbitrary units (%)
60
50
40
30
20
10
0
***
***
**
**
**
***
Day 1
Day 3
Day 7
Reference
Ti-1-450-150
Ti-1-500-150
Ti-2-400-100
Ti-2-400-150
Ti-2-450-100
Ti-2-500-150

Figure 13

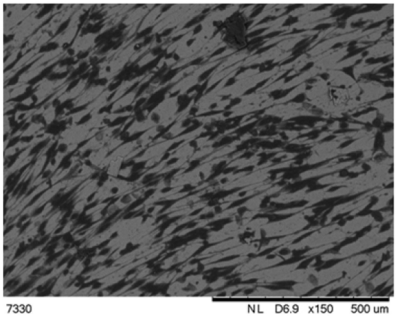

Ti-1-450-150

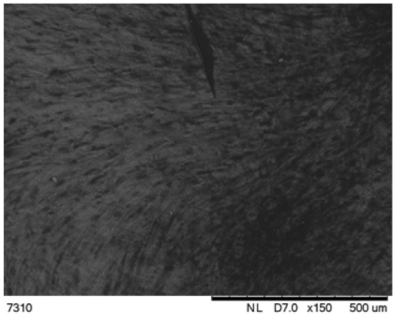

Ti-1-500-150

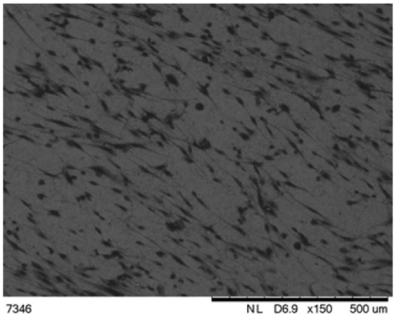

Ti-2-400-100

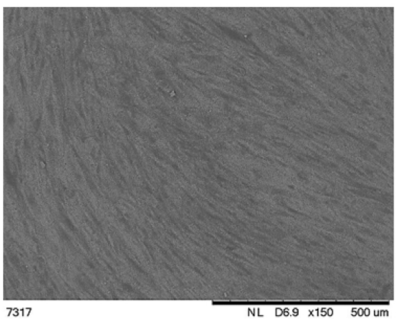

Ti-2-450-100

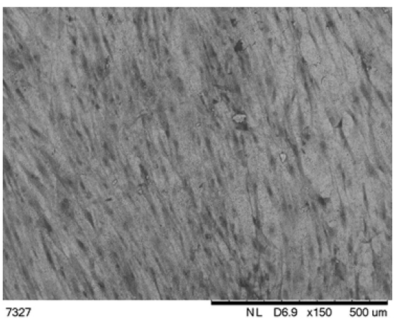

Ti-2-400-150

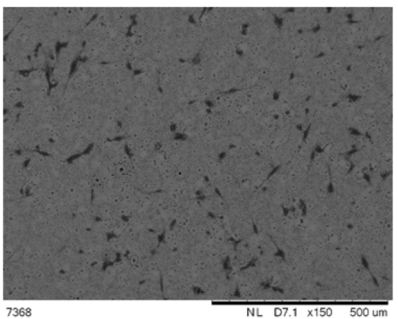

Ti-2-500-150

Figure 14

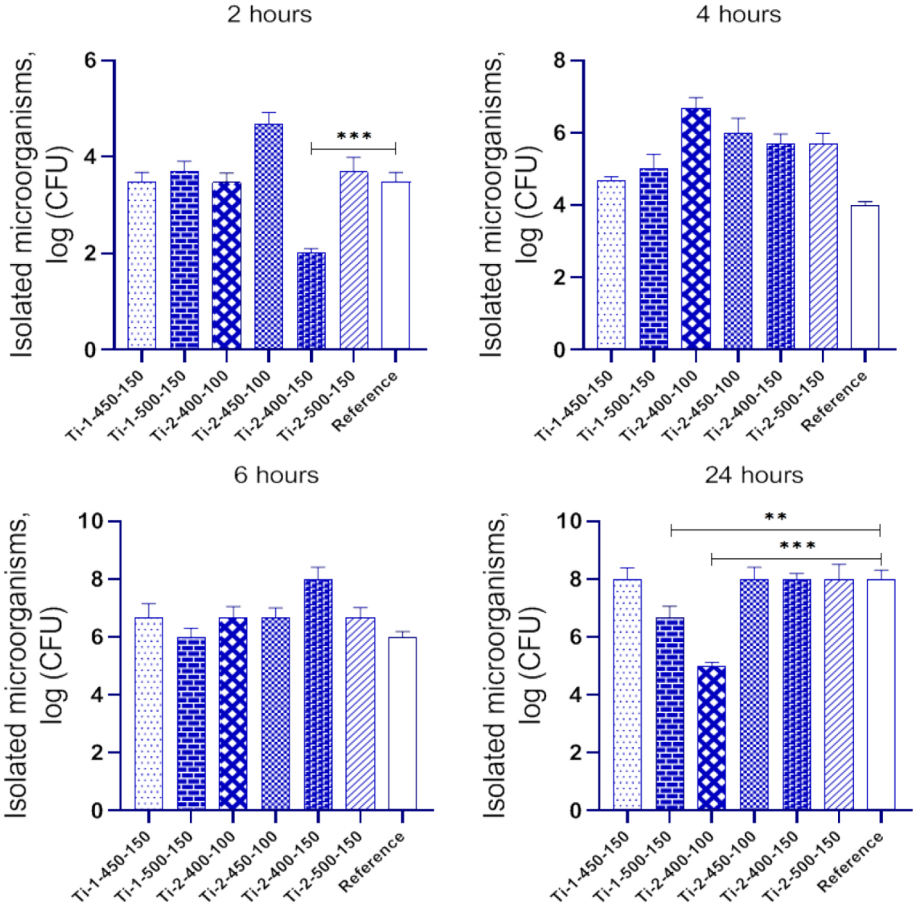
2 hours
4 hours
6 hours
24 hours
Isolated microorganisms, log (CFU)
***
**
Ti-1-450-150
Ti-1-500-150
Ti-2-400-100
Ti-2-450-100
Ti-2-400-150
Ti-2-500-150
Reference

Figure 15